Quantitative analysis of anaerobic oxidation of methane (AOM) in marine sediments: A modeling perspective

P. Regnier [a,b,*], A.W. Dale [c], S. Arndt [b,d], D.E. LaRowe [b,e], J. Mogollón [b], P. Van Cappellen [b,e]

[a] Dept. of Earth & Environmental Sciences, Université Libre de Bruxelles, Bruxelles, Belgium
[b] Department of Earth-Sciences, Utrecht University, Utrecht, The Netherlands
[c] IFM-GEOMAR Leibniz Institute of Marine Sciences, Kiel, Germany
[d] Laboratoire des Mécanismes et Transferts en Géologie (LMTG), Observatoire Midi-Pyrénées, Toulouse, France
[e] School of Earth and Atmospheric Sciences, Georgia Institute of Technology, Atlanta, GA, USA

ARTICLE INFO

ABSTRACT

Recent developments in the quantitative modeling of methane dynamics and anaerobic oxidation of methane (AOM) in marine sediments are critically reviewed. The first part of the review begins with a comparison of alternative kinetic models for AOM. The roles of bioenergetic limitations, intermediate compounds and biomass growth are highlighted. Next, the key transport mechanisms in multi-phase sedimentary environments affecting AOM and methane fluxes are briefly treated, while attention is also given to additional controls on methane and sulfate turnover, including organic matter mineralization, sulfur cycling and methane phase transitions. In the second part of the review, the structure, forcing functions and parameterization of published models of AOM in sediments are analyzed. The six-orders-of-magnitude range in rate constants reported for the widely used bimolecular rate law for AOM emphasizes the limited transferability of this simple kinetic model and, hence, the need for more comprehensive descriptions of the AOM reaction system. The derivation and implementation of more complete reaction models, however, are limited by the availability of observational data. In this context, we attempt to rank the relative benefits of potential experimental measurements that should help to better constrain AOM models. The last part of the review presents a compilation of reported depth-integrated AOM rates (ΣAOM). These rates reveal the extreme variability of ΣAOM in marine sediments. The model results are further used to derive quantitative relationships between ΣAOM and the magnitude of externally impressed fluid flow, as well as between ΣAOM and the depth of the sulfate–methane transition zone (SMTZ). This review contributes to an improved understanding of the global significance of the AOM process, and helps identify outstanding questions and future directions in the modeling of methane cycling and AOM in marine sediments.

© 2011 Elsevier B.V. All rights reserved.

Contents

---

* Corresponding author at: Dept. of Earth & Environmental Sciences, Université Libre de Bruxelles, Bruxelles, Belgium.
E-mail address: pregnier@geo.uu.nl (P. Regnier).

1. Introduction

Anoxic marine sediments are the largest methane reservoir on Earth. They contain on the order of 5000 Gt of methane carbon (Buffett and Archer, 2004), which represents 4 to 8 times the carbon in the living surface biosphere and soils combined (Kvenvolden, 1993). Geochemical (Hoehler et al., 1994; Borowski et al., 1996) and microbiological evidence (Boetius et al., 2000), together with mass balance calculations (Reeburgh, 2007), nonetheless suggest that up to 90% of the methane produced globally in marine sediments (380 Tg $CH_4 yr^{-1}$; Reeburgh, 2007) is consumed in situ before reaching the seafloor by a process known as the anaerobic oxidation of methane (AOM). Marine sediments in general and AOM in particular are thus major components of the global carbon and methane cycles with far-reaching implications for ocean biogeochemistry and earth's climate. One current concern is the possibility of a future increase in the methane release from marine sediments, which would contribute to the ongoing global climate change due to the high potential of methane for the trapping of infrared radiation.

Methane dynamics and AOM can ultimately be traced back to the process of organic matter degradation. In marine sediments the deposited organic matter is the principal energy source fueling microbial activity. This activity results in a characteristic distribution of redox conditions due to the sequential utilization in the order of decreasing Gibbs energy yield of the principal terminal electron acceptors, (TEAs) O_2, NO_3^-, Mn(III, IV), Fe(III), and SO_4^{2-} (Fig. 1).

Because organic matter and TEAs are generally supplied together at the sediment–water interface, conditions become increasingly reducing with increasing depth below the sediment surface as the available TEAs are depleted. When all external TEAs are consumed, the remaining organic matter is degraded fermentatively and releases methane and carbon dioxide to the porewaters. Organic matter degradation produces reduced aqueous compounds that migrate upwards in the sediment column and react with oxidants in the so-called secondary redox reactions (Fig. 1). In addition to the microbially driven degradation of organic compounds and secondary redox-reactions, transport processes, including advection, diffusion and biologically-induced mixing in the top-layers of the sediment, and shape sediment redox zones (Fig. 1). Although the redox zonation is a common feature of marine sediments, the depth scales over which it develops may vary by several orders of magnitude from the centimeter scale to hundreds of meters, depending on the relative magnitudes of reaction and transport rates (Fig. 1).

AOM, defined in Fig. 1 as a secondary redox reaction, can be described as the net reaction between seawater sulfate and methane:

$$CH_{4(aq)} + SO_4^{2-} \rightarrow HCO_3^- + HS^- + H_2O_{(l)} \tag{1}$$

The consumption of methane by AOM in marine sediments tends to be focused in a relatively narrow zone, the so-called sulfate–methane transition zone (SMTZ, Fig. 1), defined as the depth interval where non-zero methane and sulfate concentrations overlap (Barnes and

Primary redox*	ΔG_r^0 $J/(^1/_6 \ mol \ glucose)^{-1}$
1. Aerobic respiration $C_6H_{12}O_6 + 6O_2 \rightarrow 6CO_2 + 6H_2O$	-487046
2. Denitrification $5C_6H_{12}O_6 + 24NO_3^- \rightarrow 6H^+ + 12N_2 + 30HCO_3^- + 12H_2O$	-433160
3. Iron oxide reduction $C_6H_{12}O_6 + 24(Fe(OH)_3 + 42H^+ \rightarrow 24Fe^{2+} + 6HCO_3^- + 36H_2O$	-263606
4. Sulfate reduction $C_6H_{12}O_6 + 3SO_4^{2-} \rightarrow 3H_2S + 6HCO_3^-$	-76017
5. Methanogenesis $C_6H_{12}O_6 \rightarrow 3CO_2 + 3CH_4$	-57559

Secondary redox*
I. Nitrification
II. Fe^{2+} oxidation
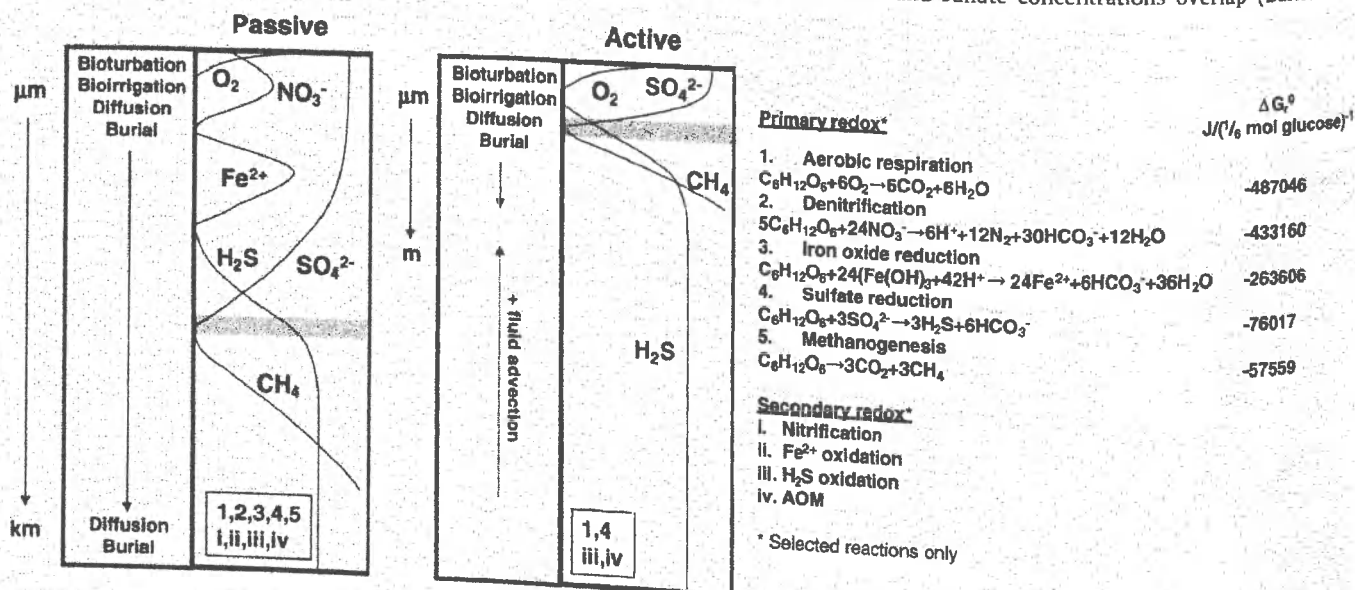III. H_2S oxidation
iv. AOM

* Selected reactions only

Fig. 1. Schematic representation of the biogeochemical zonation in marine sediments along passive and active margins (modified from Jørgensen and Kasten, 2006). The major solute and solid transport processes with increasing sediment depth are also identified. The standard state Gibbs energies of the dominant reactions involved in the oxidation of organic matter (represented as glucose, $C_6H_{12}O_6$) and major secondary redox reactions are listed on the right hand side. The most important reactions to consider for each system type are indicated in the panels by the Arabic and Roman numerals. The shaded band denotes the SMTZ and the depth scale is intended to show that the diagenetic redox sequence is tightly compressed in active margins but extends over greater depths in passive settings.

Goldberg, 1976). AOM is a microbially mediated process thought to be carried out by a symbiotic association of two types of microorganisms, methane oxidizing archaea and sulfate reducing bacteria (Hoehler et al., 1994; Hinrichs et al., 1999; Boetius et al., 2000). Alternative pathways of AOM coupled to the reduction of nitrate and iron instead of sulfate have also been reported (Raghoebarsing et al., 2006; Beal et al., 2009). However, in marine sediments where sulfate concentrations are several orders of magnitude higher than those of the alternative TEAs, methane rarely bypasses the SMTZ and these alternative pathways tend to be quantitatively far less significant. For this reason, the focus of this study is on methane oxidation coupled to sulfate reduction.

As discussed in further detail below, the depth of the SMTZ depends on many environmental factors among which externally-impressed upward fluid flow is of critical importance. Upward fluid flow compresses the SMTZ and moves it closer to the sediment surface. Sediments where fluid flow plays a major role are defined as 'active' settings in Fig. 1. With high fluid advection rates, sulfate concentrations fall to near-zero values within a few cm below the sediment–water interface. In the absence of upward fluid advection ('passive' settings, Fig. 1), the SMTZ tends to be located at much greater depth below the sediment surface. Along the continental slope, for example, the SMTZ may be at depths of up to 100 m or more (Borowski et al., 1999). Even at these great depths microorganisms remain active (D'Hondt et al., 2004; Parkes et al., 2005), although the corresponding AOM rates are orders of magnitude lower than on the shelf or in sediments with fluid flow (D'Hondt et al., 2002; D'Hondt et al., 2004). Despite the exceedingly low rates, recent studies have shown that AOM may represent the dominant sink for sulfate in deep-seated marine sediments (D'Hondt et al., 2002; Arndt et al., 2006).

Quantitative modeling approaches of varying degrees of complexity have been applied to quantify rates of AOM in marine sedimentary environments. At the lower end of the spectrum, calculated porewater diffusion fluxes based on measured vertical porewater sulfate concentration profiles afford reasonably accurate estimates of the depth integrated rate of AOM, assuming that the reactants are consumed in a 1:1 ratio (Eq. (1)). However, this approach implicitly assumes that (i) molecular diffusion is the only transport process, (ii) AOM is the only process consuming sulfate within the SMTZ, and (iii) the measured concentration profile is at steady state. In reality, one or more of these conditions are often not met. More sophisticated modeling approaches that explicitly describe the transport and reaction processes affecting sulfate and methane are then required. For simple formulations of the AOM reaction rate, the resulting differential equations can sometimes be solved analytically (Berner, 1980; Devol et al., 1984). However, it is increasingly recognized that AOM is part of an extensive biogeochemical reaction network. In particular, the sulfur cycle is exceptionally convoluted due to its intimate links with the cycles of all other major redox elements (Jørgensen and Kasten, 2006). One must, therefore, rely on more sophisticated models to identify and quantify the sources and sinks of sulfate that may not be obvious from a visual inspection of the measured concentration profile of sulfate alone (Dale et al., 2009a). To represent highly coupled reaction networks, the use of multi-component reaction-transport models (RTMs) and numerical solutions become necessary (Regnier et al., 2002). Several excellent sources on the numerical aspects of modeling coupled transport and reaction in porous media are available for the interested reader (e.g. Steefel and MacQuarrie, 1996; Boudreau, 1997) and are therefore not addressed in detail here.

Quantifying methane sources and sinks is currently at the forefront of research because of the important roles of methane and AOM in past, present and future climate changes. RTMs are well-established diagnostic tools that can be used to identify outstanding knowledge gaps. They are also particularly well suited to assess the environmen-

Table 1
Definition of variables and parameters used in the modeling of AOM. Typical units are also provided.

Parameter	Definition	Units
System description		
V	Volume (total)	cm^3, dm^3, m^3
[]	Concentration of substrate	$mol\ V^{-1}$
B	Microbial biomass	$cell\ V^{-1}$
Sal	Salinity	unitless
T	Temperature	°C; K
P	Pressure	Pa; bar
pe	$-\log(a_{e^-})$	Unitless
pH	$-\log(a_{H^+})$	Unitless
Kinetics		
t	Time	s; d; y
R_n	Rate of the nth chemical reaction	$mol\ V^{-1}t^{-1}$
$v_{max,n}$	Maximum rate of the n th reaction	$mol\ V^{-1}t^{-1}$
μ_n	Maximum specific growth rate constant by the nth catabolic reaction	t^{-1}
μ_e	Maximum specific decay rate constant by the nth catabolic reaction	t^{-1}
k_n	Rate constant of the nth chemical reaction	Variable
K_M	Michaelis–Menten constant	$mol\ V^{-1}$
Y	Microbial growth yield	$g\ biomass\ (g\ E_D)^{-1}$[*]
Thermodynamics		
K	Equilibrium constant	Unitless
ΔG_r^0	Standard state Gibbs energy of reaction	$J\ mol^{-1}$
ΔG_r	Gibbs energy of reaction	$J\ mol^{-1}$
$\Delta G_r'$	Biochemical standard state Gibbs energy of reaction	$J\ mol^{-1}$
ΔG_{BQ}	Minimum energy required for microbial growth	$J\ mol^{-1}$
Q	Reaction quotient	Unitless
v_i	Stoichiometric coefficient of the ith species	Unitless
a_i	Activity of the i th species	Unitless
γ_i	Activity coefficient of the ith species	$V\ mol^{-1}$
R	Gas constant	$J\ K^{-1}mol^{-1}$
χ	Average stoichiometric number	Unitless

[*] E_D stands for electron donor.

tal controls on the efficiency of AOM. The mechanistic nature of RTMs further allows one to predict the response of sediment biogeochemistry to periodic and secular changes in environmental forcings. The latter include, but are not limited to, seasonal variations in temperature (Dale et al., 2008a), abrupt shifts in macroscopic aqueous transport regimes (Luff and Wallmann, 2003; Dale et al., 2008b; Reagan and Moridis, 2008), turbidite events (Hensen et al., 2003), or changes in sediment and organic matter accumulation rates over geological time scales (Arndt et al., 2009). Nonetheless, numerous uncertainties remain due to the lack of time-series data of sufficient resolution and time span to characterize the environmental conditions at the seafloor.

Here, we review how recent model developments, including improved representations of the physical, chemical and biological components of the benthic system, have provided novel insight into the system-scale role of AOM under both steady state and non-steady state conditions. To our knowledge, this is the 8th review paper (book chapters and abstracts excluded) dedicated to the subject of AOM in marine sediments (Zehnder and Brock, 1980; Valentine and Reeburgh, 2000; Kotelnikova, 2002; Valentine, 2002; Strous and Jetten, 2004; Caldwell et al., 2008; Knittel and Boetius, 2009) since the existence of AOM was first postulated over three decades ago (Claypool and Kaplan, 1974; Reeburgh, 1976; Barnes and Goldberg, 1976; Martens and Berner, 1977; Reeburgh, 1980). The present review paper, however, is the first one dedicated exclusively to summarizing the efforts that have been made to quantify AOM through modeling. We begin by identifying and comparing alternative formulations for the coupled transport and reaction processes that are required to quantify AOM in contrasted sedimentary settings. We then analyze the structure, forcings and parameterization of existing RTMs as well as their capability for extrapolating AOM rates across time and spatial scales. Finally, on the

basis of more than 50 published AOM model applications, we quantify depth-integrated AOM rates across the full spectrum of environmental conditions encountered at the seafloor.

2. Methane and sulfate dynamics

2.1. The AOM reaction system

This section reviews the variety of kinetic model formulations for AOM which can be found in the literature. The simplest formulations are empirical rate equations that only depend on the concentrations of the initial reactants which, according to the net reaction in Eq. (1), are methane and sulfate. More advanced kinetic models are based on more detailed descriptions of the metabolic reaction pathways and account for the role of reaction intermediates. By explicitly representing cellular synthesis, the models can further couple the utilization of substrates to the growth of microbial biomasses. A glossary of model parameters and respective units is provided in Table 1.

2.1.1. Biogeochemical models

The simplest phenomenological expression describing the macroscopic rate of AOM, R_{AOM}, is

$$R_{AOM} = k \cdot [CH_4] \cdot \left[SO_4^{2-} \right] \tag{2}$$

where k is an apparent rate constant and square brackets refer to concentrations. One reason for the widespread use of Eq. (2) is that it only involves one adjustable parameter, k, and therefore it is easily fitted to measured porewater profiles of sulfate and methane. The bimolecular rate expression for microbially-mediated redox reactions in sediments has also been justified on theoretical grounds (Van Cappellen and Gaillard, 1996). In particular, it restricts the occurrence of the reaction to those areas in the sediment where non-zero concentrations of the electron acceptor and electron donor overlap.

The consumption of substrates by microorganisms generally exhibits saturation kinetics that is captured by the Michaelis–Menten model for enzymatically-catalyzed reactions (Regnier et al., 2005). That is, with increasing concentration of a substrate, such as methane and sulfate, the rate ultimately reaches a maximum value, ν_{max}, provided that the microbial biomass or enzyme concentration is time-invariant. At this point, all available enzymes are actively involved in substrate conversion. The substrate concentration at which the rate equals half of ν_{max} is referred to as the half-saturation constant, K_m, which is a measure of the affinity of a particular enzyme for the substrate, i.e. the lower K_m is the stronger the affinity.

For AOM, saturation kinetics with respect to both the electron donor and the electron acceptor can be expressed as

$$R_{AOM} = \nu_{max} \cdot \left(\frac{[CH_4]}{K_m^{CH_4} + [CH_4]} \right) \cdot \left(\frac{[SO_4^{2-}]}{K_m^{SO_4^{2-}} + [SO_4^{2-}]} \right). \tag{3}$$

When the porewater concentrations of methane and sulfate are much less than their respective half-saturation constants, Eqs. (2) and (3) are equivalent, with

$$k = \frac{\nu_{max}}{K_m^{CH_4} \cdot K_m^{SO_4^{2-}}}. \tag{4}$$

Laboratory experiments indicate that K_m values for methane (mM range) are much higher than those for sulfate (sub-mM range) (Nauhaus et al., 2002; Wegener and Boetius, 2009). Consequently, for the concentrations of methane and sulfate typically found in the SMTZ (~1 mM), the Michaelis–Menten term for methane reduces to a pseudo-first order dependency with respect to the concentration of

methane. The same linear approximation may not be valid for the rate dependence on the sulfate concentration, however.

By catalyzing the AOM reaction (Eq. (1)), microorganisms channel the catabolic energy into metabolism and growth via intracellular synthesis of the coenzyme adenosine triphosphate (ATP). However, AOM can only proceed when the energy yield for the catabolic reaction exceeds a minimum metabolic threshold. The kinetically-limited model for AOM can be extended to account for this bioenergetic limitation through a functional dependency on the thermodynamic driving force for the reaction, which depends on the Gibbs energy yield:

$$R_{AOM} = \nu_{max} \cdot \left(\frac{[CH_4]}{K_m^{CH_4} + [CH_4]} \right) \cdot \left(\frac{[SO_4^{2-}]}{K_m^{SO_4^{2-}} + [SO_4^{2-}]} \right) \cdot \left(1 - exp\left(\frac{\Delta G_r + \Delta G_{BQ}}{\chi RT} \right) \right)$$
$$= \nu_{max} F_K F_T \tag{5}$$

where ΔG_r is the Gibbs energy of the AOM reaction (Eq. (1)), ΔG_{BQ} is the minimum energy required to sustain ATP synthesis, χ is the average stoichiometric number of the reaction (Jin and Bethke, 2005), and R and T are the gas constant and absolute temperature, respectively. The terms F_K and F_T in Eq. (5) are abbreviations for the kinetic and thermodynamic driving forces for AOM, which are discussed below. For catabolic reactions, χ corresponds to the number of protons translocated across the cell membrane per formula reaction. Although the latter has not been directly determined for most environmentally relevant catabolic processes, χ is usually assumed to be equivalent to the number of electrons transferred per formula reaction. This assumption has also been used when modeling AOM rates in sediments (Dale et al., 2008c). The Gibbs energy of the AOM reaction as written in Eq. (1) is given by:

$$\Delta G_r = \Delta G_r^0 + RT \ln \frac{a_{HS^-} \cdot a_{HCO_3^-} \cdot a_{H_2O}}{a_{CH_4} \cdot a_{SO_4^{2-}}} \tag{6}$$

where a represents the activity of the corresponding species and ΔG_r^0 is the standard Gibbs energy of the reaction calculated from the standard molal thermodynamic properties of the chemical compounds involved in the AOM reaction (Table 2). In order for AOM to proceed, $\Delta G_r + \Delta G_{BQ}$ must be negative. Because ΔG_{BQ} is defined as a positive (energy-requiring) value, the absolute in situ magnitude of ΔG_r must exceed that of ΔG_{BQ}. Therefore, through Eqs. (5) and (6), the accumulation of reaction products limits R_{AOM} in the Thermodynamic–Kinetic model via the effect on the Gibbs energy of reaction.

The low Gibbs energy yields that have been reported for AOM in a variety of depositional environments imply that the bioenergetic limitation must be accounted for to adequately describe AOM kinetics (Hoehler et al., 1994; Knab et al., 2008; LaRowe et al., 2008). ΔG_{BQ} is on the order of 15–20 kJ per mol of electron donor for *Escherichia coli*, which allows for the synthesis of 1/3 to 1/4 moles of ATP (Schink, 1997). The reported ΔG_{BQ} values have been measured under optimal laboratory conditions, however (Schink, 1997). Most likely, microorganisms in natural settings are able to synthesize ATP for catabolic energy yields substantially below 15–20 kJ per mol of electron donor (Hoehler, 2004). It is also important to note that the energy required to synthesize ATP itself can vary widely as a function of temperature, pressure, pH, solution composition and substrate limitation (LaRowe and Helgeson, 2007).

Even for a constant value of ΔG_{BQ}, the maximum number of moles of ATP synthesized per mol of methane oxidized may not be constant. This is illustrated in Fig. 2 for the measured porewater composition from sediments at a station in the Black Sea. The amount of ATP that can be produced per electron transferred in this reaction increases as a function of the sediment depth because the Gibbs energy released by the net AOM reaction also varies with the depth. The thermodynamic constraint placed on AOM through ΔG_{BQ} may also explain the

observed methane tailing above the SMTZ where methane concentrations are too low to produce a favourable thermodynamic drive for AOM (Dale et al., 2008c). As a result, methane diffuses up from the SMTZ towards the sediment–water interface without being oxidized by sulfate, although the latter is present in abundance (Fossing et al., 2000; Jørgensen et al., 2001; Treude et al., 2005; Dale et al., 2008c; Knab et al., 2009).

The sensitivity of the rate of AOM to ΔG_{BQ} is further illustrated in Fig. 3, which shows model-predicted AOM rates using the porewater methane and sulfate concentrations measured in a sediment core in Eckernförde Bay in the Baltic Sea (Mogollón et al., 2009). The results clearly show that the calculated AOM rates are always lower when a thermodynamic limitation is included. The calculated rates are also strongly dependent on the assumed value of ΔG_{BQ}. As ΔG_{BQ} increases, the rate of AOM decreases and the range of reactant concentrations over which AOM occurs is reduced. Given the practical difficulties associated with the experimental determination of ΔG_{BQ} for AOM, the model-based interpretation of the geochemical field data offers a promising alternative approach to narrow down the range of possible ΔG_{BQ} values. For example, the fitting of an RTM to data from two sediment cores retrieved in the Skaggerak yielded estimates of ΔG_{BQ} for AOM on the order of 11 kJ (mol CH_4)$^{-1}$.(Dale et al., 2008c).

Table 2
Summary of the standard molal thermodynamic properties (at 298 K and 1 bar) for species involved in early diagenetic reactions.

Species	ΔG_f^{0a}	Species	Formula	ΔG_f^{0a}
H^+	0	HPO_4^{2-e}		−1,089,137
$H_{2(aq)}^b$	17,723	PO_4^{3-e}		−1,018,804
$O_{2(aq)}^b$	16,544	MnO_2^m		−465,140
H_2O^c	−237,178	Mn^{2+e}		−230,538
$CH_{4(aq)}^d$	−34,451	Mg^{2+e}		−453,985
$CH_{4(g)}^d$	−50,405	ATP^{4-n}	$C_{10}H_{12}N_5O_{13}P_3^{4-}$	−2,749,047
$CO_{2(aq)}^b$	−385,974	$HATP^{3-n}$	$C_{10}H_{13}N_5O_{13}P_3^{3-}$	−2,792,979
CO_3^{2-e}	−527,983	H_2ATP^{2-n}	$C_{10}H_{14}N_5O_{13}P_3^{2-}$	−2,818,920
HCO_3^{-e}	−586,940	H_3ATP^{-n}	$C_{10}H_{15}N_5O_{13}P_3^{-}$	−2,830,217
$CHOOH_{(aq)}^{d,f}$	−372,301	H_4ATP^n	$C_{10}H_{16}N_5O_{13}P_3$	−2,838,844
$COOH^{-d,g}$	−350,879	$MgATP^{2-o}$	$MgC_{10}H_{12}N_5O_{13}P_3^{2-}$	−3,236,784
$CH_3COOH_{(aq)}^{d,h}$	−396,476	$MgHATP^{-o}$	$MgC_{10}H_{13}N_5O_{13}P_3^{-}$	−3,267,683
$CH_3COO^{-d,i}$	−369,322	MgH_2ATP^o	$MgC_{10}H_{14}N_5O_{13}P_3$	−3,289,461
$C_6H_{12}O_6^j$	−915,919	Mg_2ATP^o	$Mg_2C_{10}H_{12}N_5O_{13}P_3$	−3,701,179
SO_4^{2-e}	−744,459	ADP_3^{-n}	$C_{10}H_{12}N_5O_{10}P_2^{3-}$	−1,893,883
HSO_4^{-e}	−755,756	$HADP^{2-n}$	$C_{10}H_{13}N_5O_{10}P_2^{2-}$	−1,935,305
H_2S^b	−27,920	H_2ADP^{-n}	$C^{10}H^{14}N_5O_{10}P_2^{1-}$	−1,959,154
HS^{-e}	11,966	H_3ADP^n	$C_{10}H_{15}N_5O_{10}P_2$	−1,969,614
$Pyrite^k$	−160,218	$MgADP^{-o}$	$MgC_{10}H_{12}N_5O_{10}P_2^{-}$	−2,374,520
Fe^{3+e}	−17,238	$MgHADP^o$	$MgC_{10}H_{13}N_5O_{10}P_2$	−2,403,562
Fe^{2+e}	−91,504	Mg_2ADP^{+o}	$Mg_2C_{10}H_{12}N_5O_{10}P_2^+$	−2,838,011
$FeOOH_{(aq)}^l$	−423,002	$H_2NAD_{red}^o$	$C_{21}H_{29}N_7O_{14}P_2$	−2,216,432
$N_{2(aq)}^b$	18,188	$HNAD_{red}^{-o}$	$C_{21}H_{28}N_7O_{14}P_2^-$	−2,207,646
NO_3^{-e}	−110,905	NAD_{red}^{2-o}	$C_{21}H_{27}N_7O_{14}P_2^{2-}$	−2,194,257
$NH_{3(aq)}^b$	−26,706	$H_2NAD_{ox}^{+o}$	$C_{21}H_{28}N_7O_{14}P_2^+$	−2,238,900
NH_4^{+e}	−79,454	$HNAD_{ox}^o$	$C_{21}H_{27}N_7O_{14}P_2$	−2,230,114
$H_3PO_4^b$	−1,142,650	NAD_{ox}^{-o}	$C_{21}H_{26}N_7O_{14}P_2^-$	−2,216,725
$H_2PO_4^{-e}$	−1,130,266			

Acronyms: ATP—adenosine triphosphate; ADP—adenosine diphosphate; NADox— oxidized nicotinamide diphosphate; NADred—reduced nicotinamide diphosphate.
 ^a J mol^{-1}.
 ^b Shock et al. (1989).
 ^c Johnson et al. (1992).
 ^d Shock and Helgeson (1990).
 ^e Shock and Helgeson (1988).
 ^f Formic acid.
 ^g Formate.
 ^h Acetic acid.
 ⁱ Acetate.
 ^j Amend and Plyasunov (2001).
 ^k Helgeson et al. (1978).
 ^l Shock et al. (1997).
 ^m Pyrolusite, Wagman et al. (1982).
 ⁿ LaRowe and Helgeson (2006a).
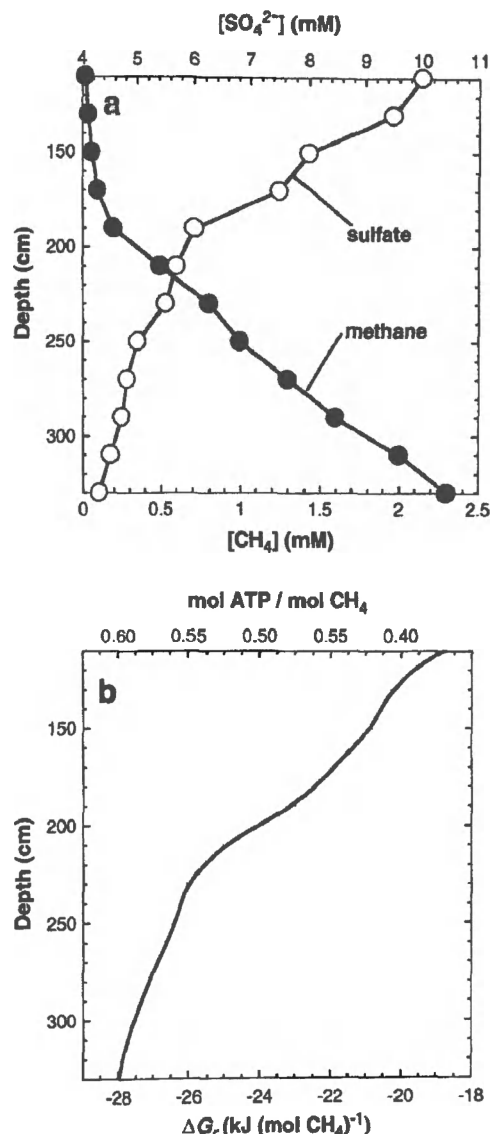 ^o LaRowe and Helgeson (2006b).

Fig. 2. Depth-dependent variation in AOM energetics: (a) concentration profiles of sulfate and methane in a Black Sea sediment core; (b) computed depth distributions of the Gibbs energy of reaction for AOM and the corresponding maximum number of moles of ATP that can be produced (b). The concentration profiles are taken from Jørgensen et al. (2001) and the energetic calculations were carried out as described in LaRowe et al. (2008). Because temperature and pressure are constant throughout the sediment section considered, the variation in AOM energetics is due to changes in chemical composition.

2.1.2. Metabolic models

A single microorganism capable of catalyzing AOM has not yet been isolated in pure culture (Knittel and Boetius, 2009). In contrast, several studies have reported a close association between methane-oxidizing archaea and sulfate-reducing bacteria in AOM environments (Orphan et al., 2001; Hinrichs and Boetius, 2002; Orphan et al., 2002). It has therefore been postulated that a consortium of microbes oxidize methane and reduce sulfate in a two-step reaction coupled through the production and consumption of reactive intermediates, such as hydrogen (H_2), formate ($HCOO^-$), and acetate (CH_3COO^-) (Hoehler et al., 1994; Valentine and Reeburgh, 2000; Sørensen et al., 2001; Nauhaus et al., 2005). Using H_2 as an example, AOM would then be represented by the following set of reactions:

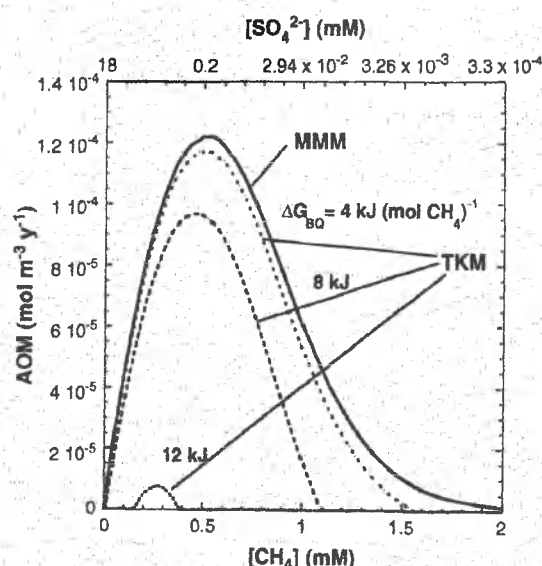$$CH_{4(aq)} + 3H_2O \rightarrow 4H_{2(aq)} \quad HCO_3^- + H^+ \tag{7}$$
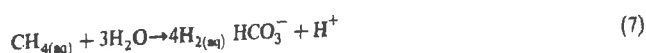
Fig. 3. Comparison of calculated AOM rates using the Michaelis–Menten model (MMM–solid curve) and the Thermodynamic-Kinetic model (TKM–dashed curves) formulations. The three TKM curves were generated using different values of ΔG_{BQ}. The K_m values for methane and sulfate were taken from Nauhaus et al. (2002) and Pallud and Van Cappellen (2006), respectively. The maximum AOM rate, v_{max}, was set to 5.5×10^{-4} (mM yr^{-1}). The standard Gibbs energy of the reaction was calculated using SUPCRT92 (Johnson et al., 1992) for the conditions prevailing at Eckernförde Bay (280 K and 3 bar). The calculations are based on the sulfate and methane concentrations measured concurrently in a core from Eckernförde Bay.

and

$$SO_4^{2-} + 4H_{2(aq)}\ H^+ \rightarrow HS_{(aq)}^- + 4H_2O. \tag{8}$$
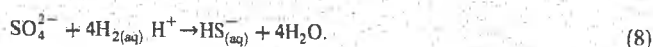
Thermodynamic calculations show that methane can only be oxidized to H_2 under a narrow range of conditions of pressure, temperature and solution composition (LaRowe et al., 2008). However, sulfate reduction coupled to the oxidation of H_2 is thermodynamically favorable over a very wide range of conditions encountered in marine sediments (LaRowe et al., 2008).

In principle, the incorporation of a reaction system such as represented by Eqs. (7) and (8) in an RTM is straightforward. It requires the addition of a new mass conservation equation for the intermediate species, H_2, while the rate expression for the net oxidation of methane by sulfate is replaced by two rate expressions, one for each of the individual reaction steps. Applications of RTMs that include metabolic intermediates of AOM have recently been presented (Dale et al., 2008c; Orcutt and Meile, 2008; Alperin and Hoehler, 2009). Results indicate that, despite the scarcity of concentration data on reactive intermediates in marine sediments, useful insights into the mechanisms and environmental controls on AOM can be gained from modeling studies. An example of RTM calculations based on reactions (7) and (8) is illustrated for a passive margin sediment in Fig. 4. The shaded area in the figure identifies the depth interval where methane is being oxidized. As shown in Fig. 4b, this corresponds to the sediment depth interval where both the kinetic (F_K) and bioenergetic (F_T) driving forces of reaction (7) are positive. The driving forces are defined as:

$$F_K = \left(\frac{[CH_4]}{K_m^{CH_4} + [CH_4]} \right) \tag{9}$$

and

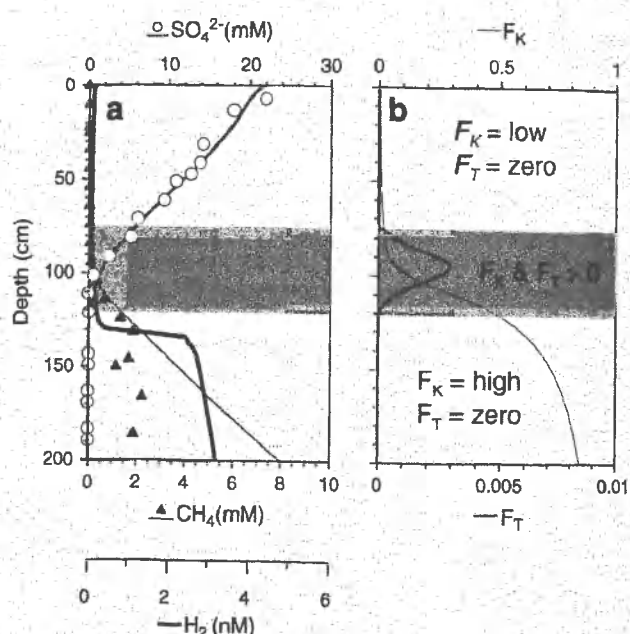$$F_T = 1 - exp\left(\frac{\Delta G_r + \Delta G_{BQ}}{\chi RT} \right) \tag{10}$$

Fig. 4. (a) Measured (symbols) and simulated (lines) profiles of sulfate and methane in a sediment core from the Skagerrak, along with the theoretical H_2 profile. The measured concentrations are taken from Dale et al. (2008c); (b) Depth distributions of F_T and F_K. See text for further details.

where the values of ΔG_r, ΔG_{BQ} and χ are those that apply to reaction (7). Above the depth interval of methane oxidation (i.e., above the SMTZ), both F_K and F_T drop to very low values because of the low methane concentrations. Below the depth interval of methane oxidation, F_K is high as a result of the build-up of methane. However, F_T approaches zero because of the accumulation of the reaction product, H_2, which in the absence of sulfate is no longer consumed via reaction (8). In other words, below the SMTZ, the oxidation of methane is limited by the insufficient bioenergetic yield of the oxidation step.

2.1.3. Biomass-explicit models

For energy yielding redox reactions that are used by microorganisms to synthesize new cell tissue, it is possible to couple the rate of consumption of the electron donor to the biomass growth (Rittmann and VanBriesen, 1996). Models in which biomasses are allowed to vary can account for the response of a microbial community to fluctuations in environmental conditions and for the competition for substrates among different microbial groups (Thullner et al., 2005). A common approach for coupling microbial population dynamics to substrate utilization is based on the Monod model. For example, the temporal change in biomass, B, of methane oxidizing archaea can be expressed as:

$$\frac{dB}{dt} = \mu_{max} \cdot B \cdot \left(\frac{[CH_4]}{K_m^{CH_4} + [CH_4]} \right) \cdot \left(1 - exp\left(\frac{\Delta G_r + \Delta G_{BQ}}{\chi RT} \right) \right) - \mu_e \cdot B \tag{11}$$

where μ_{max} (time^{-1}) and μ_e (time^{-1}) are the specific maximum growth and specific decay rates of the microbes, respectively. Although in microbial kinetics μ_{max} and μ_e are commonly referred to as specific rates, they are strictly speaking apparent rate constants. In Eq. (11) the only energy yielding reaction used by the AOM biomass is assumed to be reaction (7). A particular biomass group may rely on more than one catabolic pathway, however. In that case, the first term on the RHS of Eq. (11) is replaced by a summation over all possible catabolic pathways. The decay rate μ_e encompasses cellular loss due to death, lysis and trans-membrane leakage of metabolites. Dale et al.

(2006) proposed a μ_e value on the order of 0.1 yr^{-1} for active anaerobic methane oxidizers, although this has not been substantiated by direct experimental data.

The rate of biomass growth and substrate utilization are linked through the growth yield, Y, expressed as the amount of biomass carbon produced per unit of mass electron donor consumed. Values of Y depend on the Gibbs energy generated by the catabolic reaction, the Gibbs energy needed for the formation of a new biomass, and the efficiency with which the organisms utilize energy (VanBriesen, 2002). Yield values for AOM based on theoretical calculations (Dale et al., 2006) and laboratory experiments (Nauhaus et al., 2007) are low, typically around 0.05–0.07 mol C biomass (mol CH$_4$ oxidized)$^{-1}$. Consequently, the microbial doubling times are notably long, on the order of months to years (Nauhaus et al., 2007). This suggests that microbial AOM communities respond slowly to changes in environmental conditions and, therefore, the resolution of transient dynamics at time scales similar or shorter than that of the microbial growth may require an explicit representation of the biomass.

As an example, Fig. 5 presents simulations of AOM rates following the sudden onset of upward fluid flow in a sediment at time $t = 0$, where the SMTZ is initially located at 300 cm below the sediment surface (Dale et al., 2008b). The advection of methane-rich fluid saturates the porewater with dissolved methane and pushes the SMTZ up towards the sea floor. In the case where growth and decay of the methane-oxidizing microbial community are explicitly accounted for (Fig. 5a,b), the non-steady state effect of fluid advection is reflected in the decrease of the biomass concentration at 300 cm depth, because the sulfate required to make AOM thermodynamically favorable is no longer available. When the methane front arrives in the surface sediments where porewater sulfate is efficiently supplied by diffusion from the overlying water column, the methane oxidizers begin to grow. However, because of the slow growth kinetics, it takes up to 80 years for the biomass to reach a new steady state distribution. In the interim, methane is transported out of the sediment into the overlying ocean. In contrast, in model simulations without explicit microbial growth and decay (Fig. 5c), the AOM rate simply tracks the temporal upward movement of the methane front. In essence, these simulations assume that the AOM community adapts instantaneously to the changing conditions, resulting in a well defined SMTZ and no loss of methane to the overlying water column. These features are exemplified in Fig. 5d in which two sets of sulfate and methane profiles at $t = 25$ y are compared. Because the AOM communities are slow-growing, the biomass implicit simulations may over-estimate the efficiency of the AOM barrier during transient events of the increased fluid advection.

2.2. Transport of methane and sulfate

In this section, we review the most important transport mechanisms for sulfate and methane and their mathematical descriptions. The transport of a particulate material is briefly discussed in Section 2.4 in the context of methane hydrates and in more general terms in Section 3. Model parameters and units are identified in Table 3.

2.2.1. Aqueous transport

The advective flux of a solute d depends on the fluid advection velocity, v_a, and the local solute concentration, $[d]$. In passive environments where externally impressed fluid flow is absent, v_a is directly related to the linear sedimentation accumulation rate or sediment burial velocity, ω, which can be determined experimentally using radiotracers (e.g. Meysman et al., 2006a). Values of ω in marine sediments are highly variable and fall within the range of 10^{-5}–10^0 cm yr^{-1} (Middelburg et al., 1997), with a tendency of lower velocities with increasing water depth and distance from land. In the absence of compaction (constant porosity), v_a is equal to ω and the advective solute flux J_a is given by:

$$J_a = \omega \cdot [d] \tag{12}$$

where $[d]$ is in units of solute mass per unit total volume sediment. Porosity gradients induced by sediment compaction lead to a downward increase in v_a relative to the value at the sediment surface. The value of v_a at any depth, z, can be calculated from the porosity profile and the sediment burial velocity below the depth of compaction, ω_∞:

$$J_a = \frac{\omega_\infty \cdot \phi_\infty}{\phi_z} [d] \tag{13}$$

where ϕ_z is the porosity value at depth z, ϕ_∞ is the constant porosity below the zone of compaction, and J_a and $[d]$ are the flux and concentration values at depth z.
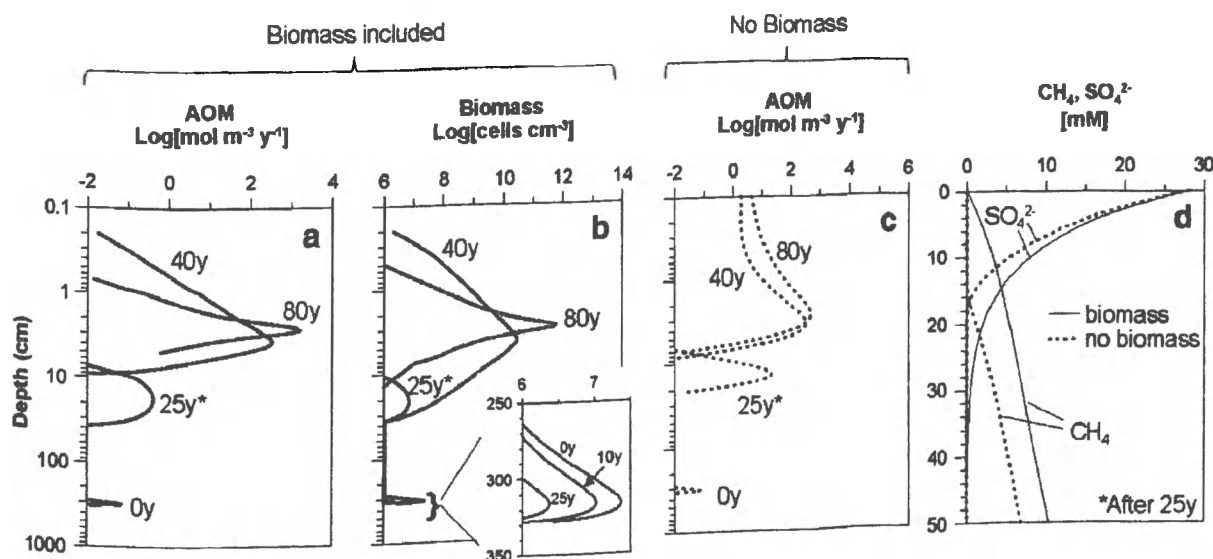

Fig. 5. Model results of a transient scenario in which an upward advective pore water flow of 10 cm yr^{-1} is imposed at the bottom of the sediment at time $t = 0$ in a system previously at steady-state with no advective flow. (a) and (b) show the AOM rate and biomass concentration for 4 time intervals using a model in which the AOM rate is dependent on the biomass concentration (Dale et al., 2008b). Steady rate is reached after approximately 80 years. (c) AOM rate predicted using the bimolecular formulation ($k_{AOM} = 10^5$ M^{-1} yr^{-1}) with no dependence on biomass concentration. (d) Model-predicted sulfate and methane concentration profiles after 25 years using the biomass implicit and explicit models. Note the presence of the decaying biomass over the first 25 years at 300 cm in panel (b), due to the relocation of the SMTZ to shallower depths after the onset of the fluid flow.

In active settings, the externally-impressed fluid flow velocity directed towards the sediment–water interface, v_{ex}, may largely exceed the burial velocity and can reach values up to several meters a year (Tryon and Brown, 2001). In this case, a simple approach consists in defining J_a as the sum of the contributions from the sediment burial and the externally-impressed fluid advection at the depth below compaction:

$$J_a = \frac{\omega_\infty \cdot \phi_\infty - v_{ex} \cdot \phi_\infty}{\phi_z} [d] \tag{14}$$

where upward flow is assigned a negative velocity. More complete treatments of advective aqueous transport combine mass and momentum balances for the aqueous and solid phases, which, in principle, allow one to simultaneously compute theoretical porosity profiles and solid and aqueous phase velocities (Maher et al., 2006; Jourabchi et al., 2010).

In a simplified representation, the flux of a dissolved species by molecular diffusion, J_d, can be approximated using Fick's First Law:

$$J_d = -D_d \cdot \frac{\partial [d]}{\partial z} \tag{15}$$

where D_d is the molecular diffusion coefficient of the solute species in the sediment, in units of the surface area total sediment per unit of time. A full treatment of diffusion in the electrolyte solutions can be found in Robinson and Stokes, 1965. The value of D_d depends on many factors including the nature of the solute species and co-occurring ions, temperature, pressure, viscosity of the fluid and ionic strength (Van Cappellen and Gaillard, 1996; Steefel and Maher, 2009). In addition, D_d must be corrected for the presence of the solid phase and reduction in porewater interconnectivity, termed tortuosity (Boudreau, 1997). The values of molecular diffusion coefficients of sulfate and methane in sediments fall in the ranges of 150–250 $cm^2 yr^{-1}$ and 200–400 $cm^2 yr^{-1}$, respectively. The variations in the diffusion coefficients mainly reflect the effects of temperature and tortuosity. The diffusive fluxes of solutes in passive settings vary by orders-of-magnitude, from values as low as $10^{-5} mol\, m^{-2} yr^{-1}$ (Arndt et al., 2009) to $10^0 mol\, m^{-2} yr^{-1}$ (Murray et al., 1978) due to widely different length scales over which concentration gradients develop.

Macrofaunal activity enhances the transport and mixing within the upper sediment layers through bioturbation and bioirrigation. These processes can increase solute exchange and impact the redox zonation. Bioturbation is the direct movement and reworking of solutes and sediment particles due to benthic fauna and is often treated as a diffusive flux, J_b, characterized by a biodiffusion coefficient

Table 3
Definition of variables and parameters relevant to transport in marine sediments. Common units are also provided.

Parameter	Definition	Units
z	Depth into the sediment	cm, dm, m
L	Length	cm, dm, m
A	Surface area (perpendicular to z)	cm^2, dm^2, m^2
V_p	Volume of the ith-phase[a]	cm^3, dm^3, m^3
ϕ_p	Pore fraction of the ith-phase[a]	V_p/V
$[d]$, $[p]$, $[g]$	Concentration of disolved, particulate and gas species	$mol\, V^{-1}$
θ	Tortuosity	(Unitless)
D_i	Molecular diffusion coefficient of the ith species	$A\, t^{-1}$
D_b	Bioturbation coefficient	$A\, t^{-1}$
v_p	Velocity of the ith-phase[a]	$L\, t^{-1}$
ω	Sedimentation rate	$L\, t^{-1}$
v_{ex}	Externally impressed flow	$L\, t^{-1}$
J_D	Diffusive flux	$mol\, A^{-1} t^{-1}$
J_g	Gaseous flux	$mol\, A^{-1} t^{-1}$
J_a	Advective flux	$mol\, A^{-1} t^{-1}$
R_i	Non-local bioirrigation flux	$mol\, A^{-1} t^{-1}$

[a] p–phases can be: g = gas, d = dissolved, p = particulate.

D_b (Berner, 1980). In the bioturbated layer, the total diffusive flux acting on solutes is thus equal to the sum of the molecular and biodiffusion fluxes $J_d + J_b$. In general, D_b increases from abyssal (10^{-2}–$10^0 cm^2 yr^{-1}$) to coastal (10^0–$10^2 cm^2 yr^{-1}$) settings due to increased macrofaunal abundances (Tromp et al., 1995; Van Cappellen and Gaillard, 1996). Biological mixing processes are difficult to quantify a priori and therefore require site-specific calibration of the bioturbation coefficient (e.g. Alperin et al., 2002).

Bioirrigation describes enhanced non-local transport of solutes across the sediment–water interface mainly by tube-dwelling organisms (Boudreau, 1984; Meysman et al., 2006b). In certain sediments, irrigation can also be caused by bubble migration through the upper centimeters of the sediment (Haeckel et al., 2007). A widely used mathematical formulation of bioirrigation assumes that the solute transfer at depth z depends linearly on the difference between the solute concentration at depth z and that at the sediment–water interface (Boudreau, 1984). The proportionality coefficient or bioirrigation coefficient varies with depth due to the size, density, and morphology of burrows and the faunal pumping rate. It also depends on the nature of the chemical species due to differences in reactivity at burrow walls (Meile et al., 2005). The order-of-magnitude estimates of bioirrigation coefficients can be obtained using the global relationships presented by Meile and Van Cappellen (2003) and Thullner et al. (2009).

2.2.2. Gaseous transport

High rates of methanogenesis can result in methane gas formation and gas overpressure, promoting sediment fracture and gas migration (Martens and Klump, 1980). Gas transport can be prevalent where vents and fractures facilitate the ascent of gas from deep methane sources, such as thermogenic gas reservoirs or hydrate dissociation (Haeckel et al., 2007). The most obvious evidence for gas transport from marine sediments is the bubble release that has been directly observed or captured by acoustic profiling (Best et al., 2006).

Simplified representations for the migration of a methane gas phase have been proposed. These include movement of the gas phase by burial through the hydrate stability zone (Davie and Buffett, 2001) and non-local transport to represent ebullition and loss from the sediment (Martens et al., 1998, Canavan et al., 2006) plus hydrate replenishment (Haeckel et al., 2004). An alternative approach treats methane gas transport as a pseudo-diffusive process where the diffusion coefficient is a fitting parameter constrained by measurements of dissolved methane concentrations and gas volume fractions (Dale et al., 2008a, 2009b). Haeckel et al. (2007) describe fast bubble rise through tube-like structures to simulate deep porewater irrigation.

The behavior of the gas phase has only recently been described in the context of multi-phase (solids, liquids, and gas) dynamics of unconsolidated marine sediments (Davie and Buffett, 2001; Mogollón et al., 2009). These models are built on the theory of momentum and mass conservation and account for the relative movement of all three phases. Similar approaches that account for an explicit gas fraction as part of a continuous 3-phase system have been widely applied to soils, aquifers, oil reservoirs and deep gas hydrate environments (e.g., Schowalter, 1979; Xu and Pruess, 2001; Molins and Mayer, 2007; Reagan and Moridis 2008; Molins et al., 2010). Generally, the gas and aqueous phases are described as continuous phases governed by Darcian flow, where the concept of relative permeability is used to describe the inhibition of the movement of one phase by the other (van Genuchten, 1980). However, the fluid flow movement occurs through a static solid matrix in these models, a limitation that precludes their direct application to shallow, gassy marine sediments which are subject to compaction, burial and particle mixing.

Mogollón et al. (2009) account for these sedimentary processes in a model for methane migration in Eckernförde Bay, where gas typically occupies a few percent of the total sediment volume. Gas

transport towards the SMTZ is simulated as a slowly-creeping continuous phase driven by buoyancy, where theoretical velocities fall within the 0–100 cm a^{-1} range. Although the direct measurement of gas ascent rates in sediments have not been reported in the literature, model results have been corroborated by comparing observed and model-derived time series of gas volume fractions (Wever et al., 1998; Mogollón et al., submitted for publication). The effect of gas migration and dissolution in their model is demonstrated in Fig. 6a, which compares depth-integrated AOM rates (ΣAOM) with model results using non-local transport to describe methane loss. As the rate of methanogenesis increases, the contribution of the gas phase to the total methane flux towards the SMTZ becomes progressively larger, leading to higher AOM rates when the gas is allowed to re-dissolve. Proportionally more sulfate is thus consumed by AOM and less is channeled into sulfate reduction coupled to organic matter oxidation (Fig. 6b), a process also thought to be operating in the continental margin of Costa Rica (Hensen and Wallmann, 2005).

Despite the potential importance of methane gas transport on AOM rates, much uncertainty still surrounds the exact mechanisms by which gas migrates through sediments. For instance, laboratory studies have shown that gas dynamics in an unconsolidated porous matrix strongly depend on the hydrodynamic regime (Stöhr and Khalili, 2006). The growth and movement of individual bubbles have also been addressed in detail (Gardiner et al., 2003; Boudreau et al., 2005; Algar and Boudreau, 2009), including their geometry and size (Anderson et al., 1998). These theoretical studies and subsequent experimentation in a gelatinous medium have led to the development of the theory of linear elastic fracture mechanics (LEFM), whereby the sediment responds elastically towards the expanding bubbles until a critical pressure threshold is reached, at which point the sediment fractures and the bubbles migrate along the fracture, potentially as a single bubble ascending at velocities near 1 cm min^{-1} (Boudreau et al., 2005). At present though, the LEFM theory remains speculative since supporting field data are lacking.

2.3. Additional controls on methane and sulfate turnover

In addition to AOM, other physical and geochemical processes, both inside and outside the SMTZ, can have a large influence on the fluxes of sulfate and methane to the SMTZ. Therefore, a complete understanding of AOM calls for the integration of this pathway into the broader biogeochemical reaction network of the sediment (Fig. 1). This section summarizes these additional processes, their mathematical description as well as their influence on AOM dynamics.

2.3.1. Organic matter degradation

As mentioned in Section 1, in passive settings organic matter synthesized in the surface waters of the ocean is the principal source of electrons from which benthic microorganisms obtain energy. The flux and reactivity of deposited organic matter influences the relative amounts of sulfate used by bacteria in organic matter degradation (organoclastic sulfate reduction) and AOM (Jørgensen and Kasten, 2006). Furthermore, enhanced burial of reactive organic matter below the sulfate reduction zone favors higher rates of methanogenesis, which in turn fuels AOM. The quantification of the production and consumption of reactive intermediates of organic matter decomposition may require consideration, as these metabolites may also be involved in AOM (e.g., H$_2$ and acetate). Although organic matter degradation exerts a fundamental control on AOM in many sedimentary environments, modeling the complex reaction pathways of organic matter degradation is a formidable challenge since some key processes are only just beginning to be sufficiently understood (Alperin et al., 1994; Burdige and Gardner, 1998; Arnosti and Holmer, 1999; Burdige et al., 2000; Hee et al., 2001; Komada et al., 2004; Jensen et al., 2005).
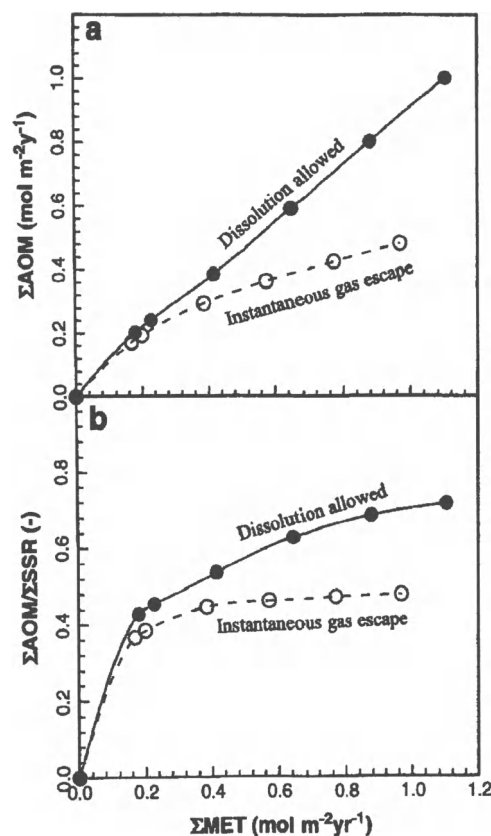

Fig. 6. (a) Depth-integrated AOM rates (ΣAOM) and (b) ratio of ΣAOM to depth-integrated total sulfate reduction rates (ΣSR) as a function of depth-integrated methanogenesis (ΣMET) for a model that includes an explicit gas phase (filled circles and solid lines), and a model where all the gas produced is instantaneously released to the water column (empty circles and dashed lines). In the gas explicit model, the dissolution of CH$_4$(g) in the SMTZ increases the AOM rate and channels more sulfate consumption into AOM at the expense of organoclastic sulfate reduction.

Natural organic matter is made of a complex mixture of high molecular weight compounds. As these compounds cannot be taken up by the cells, extracellular hydrolysis is required to produce smaller, monomeric organic molecules such as sugars and amino acids. Under anaerobic conditions, these monomers are further broken down by fermentation prior to the terminal electron-accepting step (Megonigal et al., 2004). Some studies suggest that the classical view of a slow, rate-limiting exocellular hydrolysis step of the particulate organic matter may need to be revised (Burdige and Gardner, 1998; Brüchert and Arnosti, 2003; Arnosti, 2004; Abell et al., 2009). The representation of the organic matter degradation pathway as a detailed multi-step process remains limited by the lack of appropriate reaction stoichiometries, rate expressions and kinetic parameters. In this context, scaling the kinetics of each step to the Gibbs energy yield is a possible strategy that deserves to be investigated further. For instance, Table 4 compares the standard Gibbs energies of sulfate reduction coupled to the oxidation of carbon-bearing reactive intermediates of nominal oxidation states varying from -4 (methane) to $+3$ (oxalate). Under standard state conditions, methane contains the most energy per carbon molecule whereas ethane – a compound often present in thermogenic gas mixtures – provides over 6 times less energy. Thermodynamic data may thus help constrain the relative rates at which different electron donors are utilized in anaerobic respiration. Preliminary attempts at modeling these concepts in the context of AOM have been undertaken (Dale et al., 2006, 2008a,b,c; Alperin and Hoehler, 2009).

Existing kinetic models for organic carbon degradation (R_{OC}) are primarily related to the reactivity of the macro-molecular compounds.

The 'G' model (Westrich and Berner, 1984), which has been widely used in the field of early diagenesis, assumes first-order degradation kinetics of a number of discrete organic carbon fractions, each with its own rate constant:

$$R_{OC} = \sum_i k_i \cdot [OC]_i \qquad (16)$$

where k_i and $[OC]_i$ are the rate constant and organic carbon concentration of the i-th fraction. The rate constant is usually interpreted to reflect the rate-limiting step of exo-enzymatic hydrolysis of the macromolecular organic matter constituting the corresponding fraction. However, the identification of the fractions and their corresponding reactivities is often precluded by the lack of suitable compositional and kinetic data.

Alternative approaches, in particular the power (Middelburg, 1989) and reactive continuum (Boudreau and Ruddick, 1991) models, assume a continuous distribution of reactive types. By drawing upon a large body of observational data for marine sediments, Middelburg (1989) proposed a power law dependency for the time-dependent, first-order rate coefficient k of sedimentary organic matter degradation that depends on a single parameter, the initial age, ia:

$$k(t) = 0.16(ia + t)^{-0.95} \qquad (17)$$

where k is in units of inverse years and t in units of years. Thus,

$$R_{OC} = k(t)[OC] \qquad (18)$$

The magnitude of ia is a measure of the extent of organic matter alteration during settling through the overlying water column, whereby high values of ia indicate that a larger fraction of reactive compounds has been degraded during transit. Wallmann et al. (2006b) extended the power model to include an inhibition term accounting for the influence of dissolved metabolites (methane and dissolved inorganic carbon) on particulate organic carbon degradation.

The reactive continuum model describes the bulk organic matter reactivity as the integral of an initial gamma distribution function over all possible values of k, which leads to (Boudreau and Ruddick, 1991):

$$R_{OC} = k \cdot [OC]^{1 + 1/\sigma} \qquad (19)$$

and

$$k = \frac{\sigma}{a \cdot [OC]_0^{1/\sigma}} \qquad (20)$$

The reactive continuum model requires specification of two parameters, a and σ, which together define the shape of the initial distribution of organic matter reactivity. The parameter a describes the average lifetime of the more reactive components of the spectrum,

while σ defines the shape of the distribution near $k = 0$. Low σ values reflect a predominance of unreactive types, while high σ values characterize a more uniform reactivity of the bulk organic matter pool. R_{OC} is thus a function of the initial organic matter content $[OC]_0$ and the parameters a and σ. In principle, the reactive continuum model is easier to implement than the G-model (Arndt et al., 2009). However, the G-model remains very popular because of the simplicity of its mathematical formulation.

The impact of the kinetic formulation of organic matter degradation on the magnitude of AOM rates is illustrated in Fig. 7. The depth of the SMTZ and the depth integrated AOM rate (ΣAOM) are shown as a function of organic matter reactivity, expressed in terms of ia (power model, Fig.7a), a and σ (reactive continuum model, Fig.7b) and the fraction of the less reactive organic matter pool for a 2-G model (Fig. 7c). The parameter ranges for ia, a, σ, G_1 and G_2 are representative of coastal sediments (Middelburg, 1989; Boudreau and Ruddick, 1991). Simulation results reveal that the intensity of AOM increases with a decrease in organic matter reactivity, as reflected by higher AOM rates and a shallower SMTZ (Fig. 7). This trend can be related back to the relative fractions of organic matter degradation that are channeled through sulfate reduction versus methanogenesis. High organic matter reactivity results in the near-complete consumption of organic matter within the sulfate reducing zone and, consequently, little methane production. As the reactivity decreases, an increasing fraction of the deposited organic matter is buried below the depth of sulfate penetration and more methane is produced via methanogenesis. As soon as methanogenesis begins, the upward diffusing methane triggers a shift of the SMTZ that further decreases the relative importance of organoclastic sulfate reduction, hence providing a positive feedback on AOM. This is demonstrated in Fig. 7a by the sudden change in SMTZ depth over a narrow range of ia between 9 and 11 years. Although all applied model formulations result in similar trends, the simulations also show that the magnitude of the depth-integrated AOM rate depends on the model used to represent organic matter degradation and its parameterization. It should be noted that this choice is not independent of the data set available for a particular site. For instance, rate parameters for the multi-G approach are difficult to calibrate without in situ observations. In contrast, the mathematical formulations of the other models tend to be of more general applicability.

2.3.2. Production of sulfate above and below the SMTZ

The recycling and trapping of total free sulfide (TH_2S) in marine sediments have an influence on the availability of sulfate for AOM. Organoclastic sulfate reduction and AOM are the major sources of sulfide. Sulfide sinks include burial of mineral phases such as iron sulfide (FeS), pyrite (FeS_2) and organic sulfur. In addition, sulfide can be re-oxidized in situ, either biologically with oxygen and nitrate, or abiologically by reaction with ferric iron minerals and, to a lesser extent, oxygen. Sulfide oxidation produces a variety of sulfur compounds of variable oxidation states such as thiosulfate ($S_2O_3^{2-}$)

Table 4
Standard state Gibbs energy for the oxidation of selected organic compounds coupled to sulfate reduction. Because the compounds vary by oxidation state and carbon number, the values of ΔG_r^0 are given per mole of electron transferred per mole of carbon in each compound.

Compound	Formula	Average C Oxidation state	mol e-transfer/ (mol C/mol donor)	Sulfate reduction reaction
Methane	CH_4	(-4)	8	$CH_4 + SO_4^{2-} + 2H^+ \rightarrow CO_2 + H_2S + 2H_2O$
Ethane	C_2H_4	(-3)	7	$4C_2H_6 + 7SO_4^{2-} + 14H^+ \rightarrow 8CO_2 + 7H_2S + 12H_2O$
Ethanol	C_2H_5OH	(-2)	6	$2C_2H_5OH + 3SO_4^{2-} + 6H^+ \rightarrow 4CO_2 + 3H_2S + 6H_2O$
Butanoate	$C_4H_7O_2^-$	(-1)	5	$2C_4H_7O_2^- + 5SO_4^{2-} + 12H^+ \rightarrow 8CO_2 + 5H_2S + 8H_2O$
Acetate	CH_3COO^-	(0)	4	$CH_3COO^- + SO_4^{2-} + 3H^+ \rightarrow 2CO_2 + H_2S + 2H_2O$
Glycolate	$C_2H_3O_3^-$	$(+1)$	3	$4C_2H_0O_3^- + 3SO_4^{2-} + 10H^+ \rightarrow 8CO_2 + 3H_2S + 8H_2O$
Formate	$HCOO^-$	$(+2)$	2	$4HCOO^- + SO_4^{2-} + 6H^+ \rightarrow 4CO_2 + H_2S + 4H_2O$
Oxalate	$COOHCOO^-$	$(+3)$	1	$4COOHCOO^- + SO_4^{2-} + 6H^+ \rightarrow 8CO_2 + H_2S + 4H_2O$

and elemental sulfur (S^o), which can be disproportionated to sulfate and sulfide, oxidized directly to sulfate or buried without further reaction (Jørgensen and Kasten, 2006). The relative significance of these sinks is dependent on the amount of sulfide produced, whereby low amounts of sulfide can be trapped and buried as solid sulfide before encountering oxygen or nitrate in the upper sediment layers (Fig. 1). With increasing rates of sulfide production, sulfur burial becomes comparatively less important than sulfide oxidation by microorganisms living at the oxic–anoxic interface (Jørgensen and Nelson, 2004). For instance, in Limfjorden (Denmark) sediments an estimated 90% of all sulfide produced is reoxidized biologically (Jørgensen, 1977). Intense sediment reworking by macrofaunal activity further favors repeated oxidation and reduction of sulfur bound in mineral phases prior to burial (Van Cappellen and Wang, 1996). In general, it is difficult to disentangle the various sulfur recycling pathways solely on the basis of observed geochemical profiles, and independent rate measurements plus diagnostic modeling are required.

The kinetics of biological sulfide oxidation are not fully understood, and most sediment modeling studies have relied on a simple bimolecular rate law with respect to sulfide and oxygen or nitrate:

$$R_{Sox} = k_{Sox}[TH_2S][O_2 \text{ or } NO_3]. \tag{21}$$

This rate expression implies that the process is ultimately limited by the availability of the reactants (Van Cappellen and Wang, 1996). As for AOM, rate expression (21) could be extended by replacing the

a - Power Model

b - Reactive Continuum Model

c - Multi-G Model

Fig. 7. Simulated AOM dynamics in a hypothetical coastal sedimentary setting. Steady state simulations were performed assuming a constant porosity ϕ of 0.8, a sedimentation rate $\omega = 0.4$ cm yr^{-1} (Middelburg et al., 1997) and an organic matter flux of 3 mol m^{-2}yr^{-1} (Middelburg et al., 1997). The depth of the SMTZ and ΣAOM are shown as a function of organic matter reactivity, expressed in terms of the initial apparent age, ia (power model), the free parameters, a and σ (reactive continuum model) and the relative fraction of the less reactive organic matter fraction (multi-G model). The parameter ranges for ia, a, σ, G_1 and G_2 are defined by parameter estimates for typical coastal sediments (Middelburg, 1989; Boudreau and Ruddick, 1991). The first order rate constants, k_1 and k_2, of the multi-G model are calculated based on the empirical k–ω relationships proposed by Tromp et al. (1995). The arrow indicates the values of increasing reactivity.

linear dependencies on the reactant concentrations by parabolic (i.e., Michaelis–Menten) ones, by explicitly representing the biomass of the sulfide oxidizers and by including bioenergetic limitation. Another approach to account for the effect of sulfur recycling on AOM dynamics is to fit porewater sulfate and sulfide profiles and extract a depth distribution of R_{Sox} without making any assumption on the form of the rate law (Fossing et al., 2000; Jørgensen et al., 2004). Even though the above rate descriptions have the merit of simplicity, the presence of sulfur intermediates ($S_2O_3^{2-}$, S^o) in and around the bacteria as well as measured isotope distributions suggest that sulfide oxidation is a multi-step process that may not in all cases be adequately captured by a single rate law (Fossing et al., 1995; Otte et al., 1999; Dale et al., 2009a).

Sediments hosting significant populations of large sulfide oxidizing bacteria such as *Thiomargarita* and *Beggiatoa* provide a clear example of how microbial sulfide oxidation can potentially affect AOM rates. These chemotropic bacteria thrive in sulfidic sediments at the oxic–anoxic interface and gain energy by using oxygen or nitrate as electron acceptor, which they draw from the overlying water column. The bacteria can completely oxidize sulfide and can therefore provide a large in situ source of sulfate (Fossing et al., 1995; Ferdelman et al., 1997; Brüchert et al., 2003; Jørgensen and Nelson, 2004), which is then available again for organoclastic sulfate reduction and AOM. Recently, the extent of this recycling loop has been quantified for sediments on the Namibian shelf where *Thiomargarita namibiensis* are abundant (Dale et al., 2009a). Model simulations provide compelling evidence that at one particular site *Thiomaragrita* oxidize up to 99% of the sulfide pool produced at high rates by organoclastic sulfate reduction ($\sim$6.1 mol m^{-2}yr^{-1}) and AOM ($\sim$0.2 mol m^{-2}yr^{-1}). Sensitivity studies reveal that in the absence of *Thiomaragrita*, sulfate penetration into the sediment would dramatically decrease causing an upward shift of the SMTZ thereby increasing the likelihood of methane escape (Fig. 8). The efficiency of sulfur recycling by *Thiomargarita* could thus explain the variable depth of free methane gas observed throughout the mud belt of the Namibian shelf (Emeis et al., 2004) as well as the strength and frequency of sulfide emissions from the sediment (Lavik et al., 2009).

In some settings, sulfate can be supplied to the sediments below the SMTZ by the dissolution of minerals such as barite or by the intrusion of brines from tectonically active margins. For instance, deep-seated (200–500 mbsf) Cretaceous black shales at Demerara Rise are enriched in biogenic barite (Arndt et al., 2006; Arndt et al., 2009). AOM depletes the sulfate above the black shale sequences thereby promoting undersaturation and dissolution of barite below the SMTZ, and supplying sulfate to the porewater (Arndt et al., 2006). In deep sediments of the Peru margin, a deep brine incursion provides a supplementary sulfate source, leading to the appearance of two SMTZs at 30 and 90 mbsf with active microbial methanotrophes and methane accumulation in between (Parkes et al., 2005). Similarly, Hensen and Wallmann (2005) reported the existence of two SMTZs in sediments drilled in the Costa Rica forearc area. Here, the sulfate supply to the deeper SMTZ originates from subducted pore fluids. The broader quantitative significance of these deep sulfate sources remains nevertheless inconclusive but could be important locally for the methane budget of the deep biosphere.

2.3.3. Methane phase transitions

The impacts of methane hydrate and methane gas reservoirs on AOM rates depend on their location relative to the sediment–water interface (Borowski et al., 1996). Methane gas hydrates can form when the concentration of dissolved methane in the region of hydrate stability exceeds the solubility concentration (Kvenvolden, 1993). This region is defined by the phase equilibrium between dissolved, gaseous and hydrated (solid) methane and is known as the gas hydrate stability zone (GHSZ, green area in Fig. 9). The vertical extension of the GHSZ in sediments is determined by the intersection
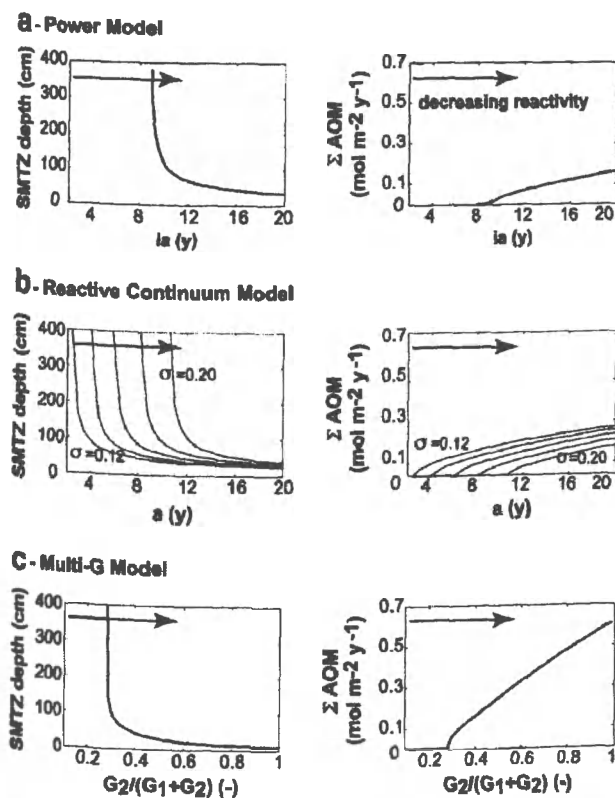
of the curve defining the local temperature, pressure (i.e. water depth) conditions (dashed line in Fig. 9) with the phase boundary delimiting dissolved methane in equilibrium with hydrate and gas (thick line). Note that other factors such as ionic strength and gas composition can also affect the width of the GHSZ (Bohrmann and Torres, 2006). Below the GHSZ, the increase in geothermal temperature shifts the dominant equilibrium state of the system from liquid + hydrate to liquid + gas. From the figure, one can deduce that hydrates are mainly located on the continental slope and rise, yet can form in very cold sediments at water depths of about 300 m such as on the Arctic shelf (Archer et al., 2008). Elsewhere, bottom water temperatures on the continental shelf are usually too high to allow the hydrate to form and a methane gas phase may be present instead. The algorithms for calculating the solubility of methane hydrate in equilibrium with dissolved methane have been proposed (e.g. Tishchenko et al., 2005). The methane concentration in equilibrium with respect to the gas phase, CH_4^*, has been extensively studied by Duan et al. (1992). A simplified algorithm based on this work has been derived for S (1–35), T (273.15–290.15 K) and P (1–30 atm) conditions encountered in continental shelf sediments (Dale et al., 2008a):

$$CH_4^* = 1.4388 \times 10^{-7} \; STP - 4.412 \times 10^{-5} TP - 4.6842 \times 10^{-5} SP$$

$$+ \; 4.129 \times 10^{-9} \; ST + 1.43465 \times 10^{-2} \; P - 1.6027 \qquad (22)$$

$$\times 10^{-6} \; T - 1.2676 \times 10^{-6} \; S + 4.9581 \times 10^{-4}$$

This algorithm can be used to calculate methane gas formation directly from the aqueous phase, a process which occurs in shallow sediments where methanogenesis rates are high and gas solubility is low.

The production of methane gas from the dissociation of hydrates right above the GHSZ provides a deep, fast rising gaseous source that could bypass the SMTZ altogether (Haeckel et al., 2007). Alternatively, the continuous consumption of methane by AOM could favor gas dissolution during its upward migration and result in a high flux of dissolved methane to the SMTZ (e.g. Haeckel et al., 2004; Mogollón

Fig. 9. General illustration of the stability field of methane hydrate in the contemporary ocean (modified after Bohrmann and Torres, 2006). The thick line is the phase boundary delimiting dissolved methane in equilibrium with hydrate and gas. In principle, hydrate is stable anywhere to the left of the phase boundary. Thus, the increase in temperature (dashed line) in the surface mixed layer of the ocean and with depth in the sediment by geothermal heating restricts the domain of the hydrate formation to the green shaded area. Intersections of the temperature profile with the phase boundary define the vertical extension of the gas hydrate stability zone (GHSZ).

et al., 2009). Model studies at Blake Ridge (site 997) and at the Costa Rica forearc (site 1040) have shown that a deep hydrate layer located around 100–200 m below the sea floor provides a distant source of dissolved methane for the SMTZ located approximately 20 m below the sea floor (Hensen and Wallmann, 2005; Wallmann et al., 2006b), a mechanism which may resemble the one depicted in Fig. 6. Near surface hydrates, which develop under conditions of highly focused advection of methane-rich pore fluid in deep waters, provide a habitat for anaerobic methanotrophs and sustain very high rates of AOM (Luff and Wallmann, 2003). Gas formation from hydrate dissociation is also thermodynamically possible directly below the GHSZ. As there is evidence for disequilibrium between hydrate and gas within hydrate-bearing sediments, gaseous and aqueous methane transport could also occur through the GHSZ (Flemings et al., 2003; Haeckel et al., 2004; Torres et al., 2004; Wallmann et al., 2006b). To our knowledge, the role of methane transport through hydrate layers on AOM rates has yet to be addressed.

The implementation of phase transitions into reactive-transport models requires kinetic descriptions of the rate at which methane is exchanged between the hydrate, gas and aqueous phases (Bhatnagar et al., 2007). Generally, the rate of methane transfer is assumed to depend on the degree of disequilibrium. The simplest formulation is based on a linear dependence (e.g. Haeckel et al., 2004; Hensen and Wallmann, 2005; Mogollón et al., 2009):

$$R_{pt} = k_{pt} \cdot \left(\frac{[CH_4]}{[CH_4]_{eq}} - 1 \right) \qquad (23)$$

where the term in brackets is a measure of the departure of the observed aqueous methane concentration from its equilibrium value ($[CH_4]_{eq}$) with respect to hydrate or gas (if present). Depending on the relative magnitudes of $[CH_4]$ and $[CH_4]_{eq}$, this term will act as either a source or sink of aqueous methane. The mass transfer coefficient which defines the rate of exchange between phases, k_{pt}, can take different values depending on the nature of the phases involved as well as on the direction of the phase transition. Previous studies have constrained these kinetic coefficients by fitting model results to experimental data (Haeckel et al., 2004; Hensen and Wallmann, 2005; Mogollón et al., 2009). Mogollón et al. (2009) further included
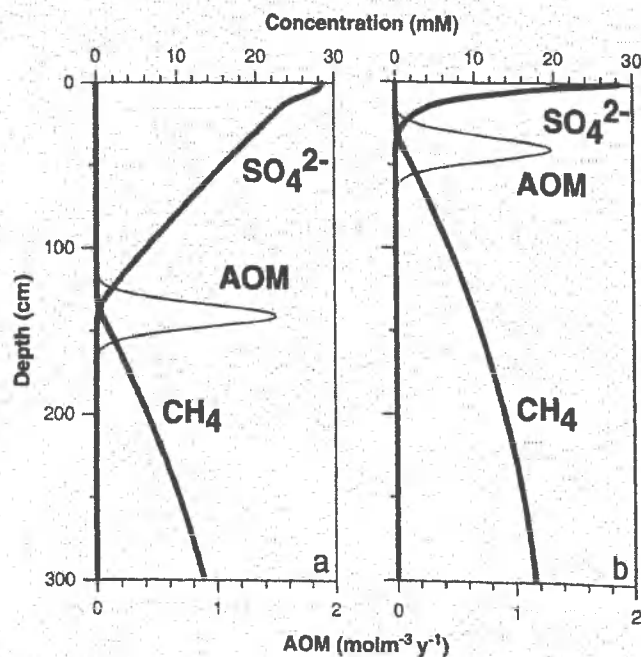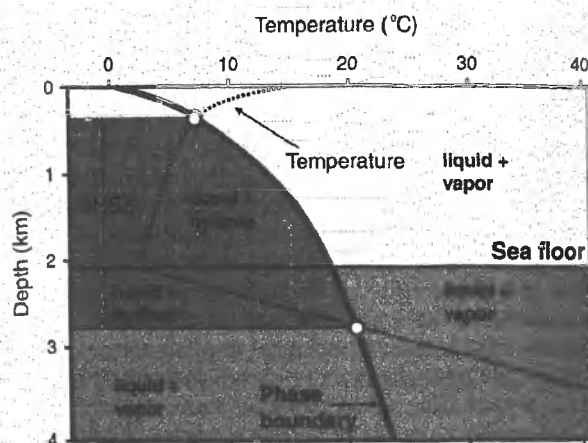

Fig. 8. (a) Representative steady-state modeled depth profiles of the AOM rate, sulfate and methane concentrations for the sediments on the inner Namibian shelf characterized by high biomasses of sulfide oxidizing *Thiomargarita* bacteria; (b) modeled profiles showing the effect of setting the rate of sulfide oxidation to zero, modified from Dale et al. (2009a).

nucleation of gas bubbles and distinguished between diffusion- and interface-controlled kinetics to describe the bubble growth and dissolution rates. Models that incorporate multiphase dynamics of hydrate, gaseous and dissolved methane transport, as well as the key biogeochemical processes, will allow us to better understand the dynamic interplay between methane transport and AOM in contrasting sedimentary environments.

3. Model formulation and implementation

3.1. Model design

This section focuses on the coupling of the reaction and transport processes discussed up to this point into a single quantitative model framework (Fig. 10). Two fundamental aspects in model design are 'support' and 'scope' (Nihoul, 1976). Support defines the physical dimension of the model and consists of time, t, horizontal (x,y) and vertical (z) dimensions, each characterized by a given span and resolution. Scope refers to the state variables and their evolution within the model support. The state variables correspond to the selected components of the solid, aqueous, gaseous and biological phases. They are coupled to one another through the various transformation processes that, together, form the biogeochemical reaction network.

A major challenge consists in choosing an optimal model representation that remains simple enough to keep the model within tractable limits, while at the same time resolves the state variables and processes that are required to describe the system adequately. Fig. 10 provides useful guidelines for the selection of the appropriate AOM model. The reduction in model complexity can be achieved by averaging the support or aggregating the scope (Nihoul, 1976). Continuum representations of the constitutive equations are based on the concept of the representative elementary volume within which homogeneous conditions are assumed (Bear, 1972). In early diagenesis, the reduction of support is often performed by integrating over the horizontal dimensions, under the assumption that the major flux and concentration gradients are vertical. However, this reduction

neglects natural horizontal heterogeneities, such as those often observed in settings with fluid and gas migration (e.g. Tryon and Brown, 2001). In addition, the vertical resolution of the model should capture the characteristic scales over which the gradients develop. The large range of rates in the field often requires a variable resolution of the model support, from the sub-millimeter scale at the sediment–water interface (Luff and Wallmann, 2003) to the meter scale in the deep biosphere (Arndt et al., 2009).

Many existing model applications assume time-invariant conditions. This approach is valid if the relaxation time of the system is significantly shorter than the characteristic timescales of fluctuations of the boundary conditions. Nevertheless, the increasing temporal resolution of observational data indicates the potential importance of transients. For instance, the AOM dynamics in coastal environments such as Aarhus Bay (Dale et al., 2008a) and Eckernförde Bay (Albert et al., 1998; Martens et al., 1998) are characterized by significant seasonal variations mainly induced by changes in the sea water temperature. The temperature not only affects microbially-mediated reaction rates, but also methane solubility and, thus, the rate of gas production and transport. On longer timescales, the scenarios of enhanced upward methane flux associated with variations in the fluid flow rates have revealed the potential importance of transient events that may allow for the methane to escape from the sediments (Dale et al., 2008b). The evolution of the organic carbon deposition flux and the chemical composition of seawater over geological timescales may also strongly influence long-term AOM dynamics (e.g. Catling et al., 2007; Arndt et al., 2009).

In terms of scope, total sediment volume conservation can only be accounted for if the phase dynamics are explicitly included in the model formulation. Phase transitions may exert an important influence on the porosity and permeability of the sediments (Steefel and Lasaga, 1994; Audet, 1995; Jourabchi et al., 2010). For instance, in active margins, high AOM rates lead to precipitation of authigenic carbonates within the SMTZ (Aloisi et al., 2004a; Luff et al., 2004). This reaction process exerts a negative feedback on the magnitude of the methane and sulfate fluxes to the SMTZ and, thus, on AOM rates. In addition, changes in gas volume due to migration and changes in temperature and pressure can only be properly simulated if phase dynamics are incorporated at the design stage (Mogollón et al., 2009).

The total number of biogeochemical variables included in an RTM depends on the choice of the AOM formulation and on the extent to which other biogeochemical processes influence methane and sulfate fluxes to the SMTZ. The constitutive equations can be implemented using different levels of dynamic approximations. The choice of alternative descriptions of the AOM reaction, transport processes, and additional controls on methane and sulfate fluxes have been discussed above. Time-dependent, one-dimensional, constitutive equations for dissolved, d, gaseous, g, or solid, p, components are, respectively,

$$\frac{\partial[d]}{\partial t} = \frac{\partial}{\partial z}(J_a + J_d + J_b) + R_i + \sum_k s_{d,k} R_k \tag{24}$$

$$\frac{\partial[g]}{\partial t} = \frac{\partial J_g}{\partial z} + \sum_k s_{g,k} R_k \tag{25}$$

$$\frac{\partial[p]}{\partial t} = \frac{\partial}{\partial z}(J_s + J_b) + \sum_k s_{p,k} R_k \tag{26}$$

where J_a, J_d, J_b, J_g and J_s are the fluxes due to porewater advection, diffusion, bioturbation, gas transport, and sediment accumulation, respectively, and R_i is the rate of solute transfer by (bio)irrigation. The summations in the constitutive equations include the rates, R_k, of all the biogeochemical processes consuming or producing the j-th component and the corresponding stoichiometric coefficients, $s_{j,k}$. For instance, for aqueous methane the summation would include its production by methanogenesis and hydrate/gas dissolution and its
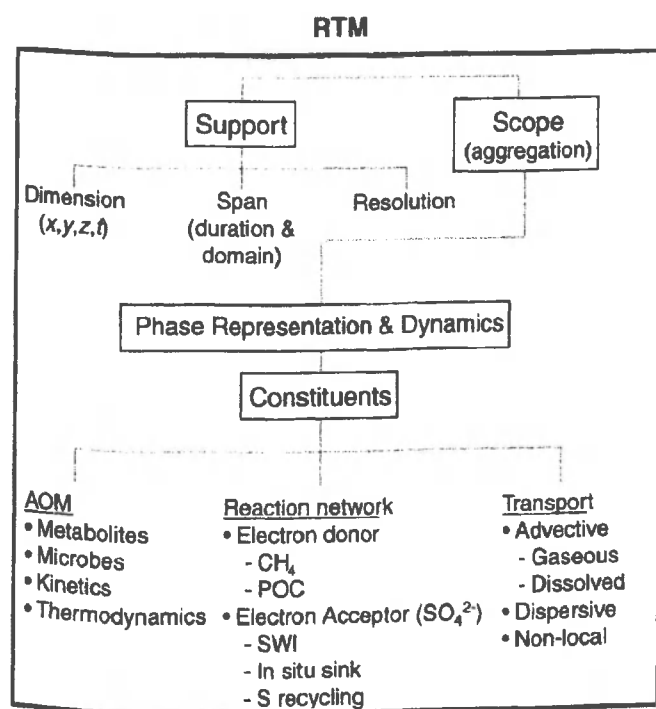
RTM

Fig. 10. Schematic representation of the multiple steps involved in the design of an AOM model.
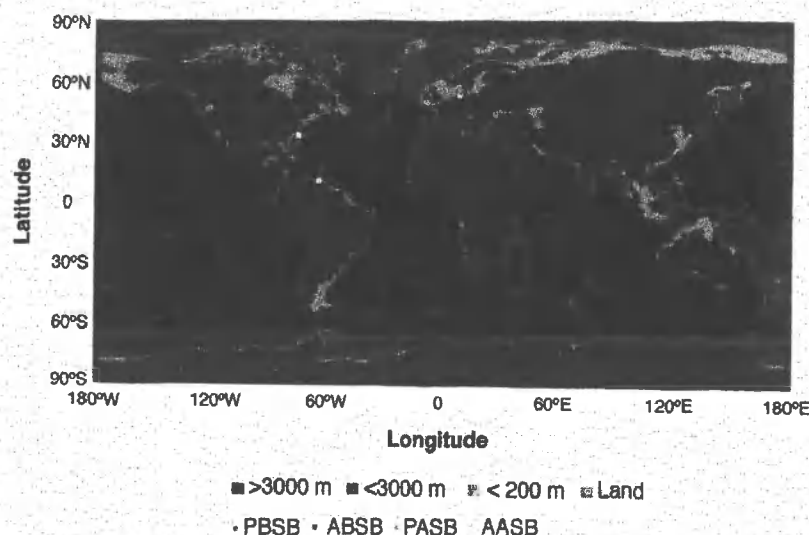
Fig. 11. Global distribution of sites at which reactive transport modeling has been applied to quantify AOM. The sites are divided into four AOM environments according to the nature of the methane flux from below and the location of the site: passive above shelf break (PASB), passive below shelf break (PBSB), active above shelf break (AASB), and active below shelf break (ABSB).

consumption by AOM and hydrate/gas formation. Note that the concentrations in the above equations are expressed per unit total sediment volume. They can easily be converted to more commonly used units, e.g., $mol\,L^{-1}$, $mol\,g^{-1}$, and volume fraction, when comparing model results with measured concentrations (e.g. Berner, 1980; Boudreau, 1997). The inclusion of microbial biomasses in the existing RTMs for AOM assumes that the microorganisms are attached to particles and can be treated as particulate components (Dale et al., 2008b). More sophisticated approaches have been proposed, which include attachment/detachment processes and biofilm formation (see Thullner et al., 2007 for a review), however these have not yet been used in the context of AOM.

The solution of the one-dimensional partial differential equations formulated above requires the specification of boundary conditions at the upper and lower model domains. The boundary conditions exert a crucial influence on the predicted spatio-temporal distributions of the state variables. Boundary conditions are typically classified as concentration (Dirichlet), gradient (Neumann) and flux (Robin) conditions. They are thoroughly reviewed by Boudreau (1997) in the context of early diagenesis. At the SWI ($z=0$), concentration conditions set to bottom water values are commonly used for the solutes and gaseous species, while a flux condition is generally imposed for the solid species:

$$-\omega \cdot [p]_0 + D_B \frac{d[p]}{dz}\bigg|_{z=0} = J_0. \qquad (27)$$

In the case that microbial biomasses are included in the model design, the corresponding upper boundary condition could be approximated as $J_0=0$, unless experimental evidence suggests otherwise. At the lower boundary ($z=L$), commonly defined at a depth where burial rates largely exceed both diffusion and local production/consumption, a zero diffusive flux condition is typically prescribed.

A zero-flux condition at the lower boundary may be unsuitable for the dissolved methane since methanogenesis often produces non-zero concentration gradients to depths well-below the modeled domain. In this case, it is customary to apply a Dirichlet condition using the measured concentrations at the lower boundary. In this context, the degassing of methane due to the drop in pressure during core recovery often prevents a direct estimation of an accurate lower boundary condition. To circumvent this problem, educated guesses can be used to infer the lower methane boundary concentration by

fitting the model to the sulfate, sulfide and alkalinity profiles which are strongly determined by the rate of AOM. Alternatively, in settings characterized by the dissociation of gas hydrates the concentration of the dissolved methane in equilibrium with gas hydrate can be imposed as a boundary condition (e.g. Luff and Wallmann, 2003). With respect to the gas phase, it is difficult to accurately measure the in situ methane gas volume and thus the specification of the boundary conditions is uncertain. In previous studies, the concentration has been fixed to low volume fractions (e.g. Dale et al., 2009b) or assumed to be zero when the model domain extends beyond the zone of gas formation (e.g. Albert et al., 1998; Martens et al., 1998, Mogollón et al., 2009).

3.2. Model parameterization and transferability

Model building is an iterative process that requires formulation and parameterization of the constitutive equations and their boundary conditions. Model parameters can be constrained through theoretical considerations or through site-specific field and laboratory observations. A comparative analysis of the AOM modeling studies applied to 61 sediment cores and 3 virtual settings provides further insight into the performance of alternative model structures and parameterizations. The locations of all sites where the cores were recovered are shown in Fig. 11; the key aspects of the formulation and kinetic constants for AOM and organic matter degradation used in the models are summarized in Table 5.

The bimolecular rate equation for AOM (Eq. (2)) forms the basis of 29 out of the 64 model applications. A first-order dependency on the methane concentration combined with either a zero-order or Michaelis–Menten dependency on the sulfate concentration is found in 7 and 5 studies, respectively, while a double Michaelis–Menten dependency on both the methane and sulfate concentrations (Eq. (3)) is used in 8 studies. In vitro slurry experiments by Nauhaus et al. (2005) imply that values of the methane half saturation constant fall in the mM range, while the half saturation constants for sulfate reducers involved in methanotrophy are similar to typical sulfate concentrations towards the base of the SMTZ (0.5 mM, Wegener and Boetius, 2009). The latter fall within the range reported for organoclastic sulfate reduction (0.1–0.9 mM, Pallud and Van Cappellen, 2006). From these data it would appear that AOM would become methane limited before it becomes limited by sulfate, although such a trend is hardly identifiable in measured AOM rates (Iversen and Jørgensen, 1985).

Table 5

Summary of AOM modeling studies. The table reports the major features of each model design. Blank entries indicate that a specific aspect of the design is not included in the model construction. The references in italics do not provide depth integrated AOM rates and are not included in Table 7. Entries in bold denote theoretical studies which are also excluded from Table 7.

Site (station name)	Location	Coordinates	AOM rate	Fluid advection	Methane gas	Bioirrigation ● Bioturbation ○	OM model type	OM degradation rate constant (y^{-1})[b]	Hydrates	Sulfur recycling	Mats	Transient	Phases	Reference
No biomass														
Bimolecular														
Anaximander Mountains	Eastern Mediteranean	34°N 25°E	10	●		●○						●	●	Aloisi et al., 2004a
Anaximander Mountains	Eastern Mediteranean	34°N 25°E	25.0	●					●					Haese et al., 2003
Derugin Bassin/ Sakhalin Island	Sea of Okhotsk	54°N 146°E	1	●		○						●		Aloisi et al., 2004b
Derugin Bassin/ Sakhalin Island	Sea of Okhotsk	54°N 146°E	$10^4 - 10^6$	●	●		2-G	$(0.02\text{-}0.1)\ 10^{-3}$, 10^{-5}				●		*Haeckel et al., 2007*
Derugin Bassin/ Sakhalin Island (SO178 3-4 KAL)	Sea of Okhotsk	48°N 146°E	0.001	●			power law		●					Wallmann et al., 2006b
Derugin Bassin/ Sakhalin Island (LV28 2-4 SL)	Sea of Okhotsk	48°N 146°E	0.001	●			2-G & power law	$0.3\ 10^{-3}$, $0.5\ 10^{-5}$	●					Wallmann et al., 2006b
Derugin Bassin/ Sakhalin Island (SO178 10-6 SL)	Sea of Okhotsk	50°N 146°E	0.03	●			power law		●					Wallmann et al., 2006b
Derugin Bassin/ Sakhalin Island (SO178 13-6 KL)	Sea of Okhotsk	53°N 145°E	0.01	●			power law		●					Wallmann et al., 2006b
Derugin Bassin/ Sakhalin Island (SO178 29-2 KL)	Sea of Okhotsk	54°N 144°E	0.001	●			power law		●					Wallmann et al., 2006b
Derugin Bassin/ Sakhalin Island (LV28 20-2 SL)	Sea of Okhotsk	54°N 144°E	0.02	●			2-G & power law	10^{-3}, $0.8\ 10^{-5}$	●					Wallmann et al., 2006b
Blake Ridge (ODP 997)	Offshore South-Eastern US	31°N 75°W	0.001	●			power law		●					Wallmann et al., 2006b
Hydrate Ridge	Cascadia Subduction Zone	45°N 125°W	0.02	●		●	2-G	$200\ 10^{-3}$, $30\ 10^{-5}$ [c]				●	●	Luff et al., 2005
Hydrate Ridge	Cascadia Subduction Zone	45°N 125°W	0.1	●		●	2-G	$200\ 10^{-3}$, $30\ 10^{-5}$ [c]					●	Luff et al., 2004
Hydrate Ridge	Cascadia Subduction Zone	45°N 125°W	0.1	●		●	2-G	$200\ 10^{-3}$, $30\ 10^{-5}$				●		Luff and Wallmann, 2003
Hydrate Ridge (BIGO 4)	Cascadia Subduction Zone	45°N 125°W	0.1[c]	●		○	2-G	$200\ 10^{-3}$, $30\ 10^{-5}$ [c]		●	●			Sommer et al., 2006
Hydrate Ridge (BIGO 5)	Cascadia Subduction Zone	45°N 125°W	0.1[c]	●		○	2-G	$200\ 10^{-3}$, $30\ 10^{-5}$ [c]		●				Sommer et al., 2006
Hydrate Ridge	Cascadia Subduction Zone	45°N 125°W	16	●								●		Zeebe, 2007
Middle America Trench	Costa Rica Forearc	10°N 86°W	0.01	●			2-G	$4\text{-}8\ 10^{-7}$, $2\text{-}23\ 10^{-9}$	●					*Hensen and Wallmann, 2005*
Middle America Trench	Costa Rica Forearc	9°N 84°W	0.5	●		○								Schmidt et al., 2005
Site 1040/1254	Costa Rica Forearc	9°N 86°E	1000	●										Haeckel, 2006
EDGE sector	Aleutian Trench	57°N 148°W	10	●		○				●				*Wallmann et al., 1997*
Dvurechenskii mud volcano (MIC - 3)	Black Sea	44°N 17°E	100	●										Wallmann et al., 2006a
Dvurechenskii mud volcano (MIC - 4, MIC - 5)	Black Sea	44°N 17°E	20	●										Wallmann et al., 2006a
Amazon Fan	Brazilian Continental Shelf	5°N 46°W	37											Blair and Aller, 1995
Eckernfoerde Bay	Kiel Bight	54°N 10°E	8.5	●	●		1-G	$10\ 10^{-3}$				●	●	Mogollón et al., submitted
Benguela Coastal Upwelling System	Namibian Shelf	22°S 12°E	10			●○	3-G	$2.0, 30\ 10^{-3}$, $14\ 10^{-5}$	●		●	●		Dale et al., 2009a

Table 5 (continued)

Site (station name)	Location	Coordinates	AOM rate	Fluid advection	Methane gas	Bioirrigation ● Bioturbation ○	OM model type	OM degradation rate constant $(y^{-1})^b$	Hydrates	Sulfur recycling	Mats	Transient	Phases	Reference
Ganos Fault	Sea of Marmara	40°N 28°E	0.1	only CH₄										Halbach et al., 2004
Santa Barbara Basin	Offshore Southwest US	34°N 120°W	10				3-G	2.0, 56 10^{-3}, 110 10^{-6}						Meysman et al., 2003
Theoretical model	Active site (theoretical)		not reported	●	●				●				●	**Bhatnagar et al., 2008**
First-order methane			y^{-1}											
Eckernfoerde Bay (Pockmark)	*Kiel Bight*	54°N 10°E	8	●	●		1-G	18 10^{-3}						Albert et al., 1998
Eckernfoerde Bay (Acoustic window)	*Kiel Bight*	54°N 10°E	8	●	●		1-G	18 10^{-3}						Albert et al., 1998
Eckernfoerde Bay	*Kiel Bight*	54°N 10°E	8	●	●		1-G	28 10^{-3}						Martens et al., 1998, 1999
Saanich Inlet	West Coast North America	48°N 123°W	44 - 57				1st order SO_4^{2-}							Devol et al., 1984
Long Island Sound	East Coast US	41°N 72°W	0.25											Martens and Berner, 1977
Cape Lookout Bight	North Carolina US	34°N 76°W	0	●			1-G	10 10^{-3}						Martens et al., 1998
Hikurangi Margin	New Zealand	42°S 175°E	30	●		●○	1-G	0		●	●			Dale et al., 2010
First-order methane, michaelis-menten sulfate			y^{-1}											
Demerara Rise	Southern Atlantic	9°N 54°W	2 - 4 x 10^{-4}				1-G	10^{-8} & 1.5-3.5 $10^{-9\ d}$						Arndt et al., 2006
Demerara Rise	*Southern Atlantic*	9°N 54°W	2 x 10^{-4}				Continuum					●		Arndt et al., 2009
Middle America Trench	Costa Rica Forearc	9°N 84°W	0 - 100; avg =3	●						●				Linke et al., 2005
Hydrate Ridge (Beggiatoa 1)	Cascadia Subduction Zone	44°N 125°W	67^e								●			Treude et al., 2003
Hydrate Ridge (Beggiatoa 2)	Cascadia Subduction Zone	44°N 125°W	67^e	●							●			Treude et al., 2003
Michaelis-menten sulfate & methane														
Eckernfoerde Bay	Kiel Bight	54°N 10°E	550	●	●		1-G	10 10^{-3}					●	Mogollón et al., 2009
North Atlantic (ODP leg162 site984A)	Reykjanes Ridge	61°N 24°W	0.471	●			1-G						●	Maher et al., 2006

			mM⁻¹y⁻¹						
No biomass									
Kinetic-thermodynamic									
Aarhus Bay (M1)	Baltic Sea	57°N 10°E	710	●○	3-G	0.22, 3.5 10⁻³, 0		●	Dale et al., 2008a
Aarhus Bay (M5)	Baltic Sea	57°N 10°E	710	●○	3-G	0.12, 0, 0		●	Dale et al., 2008a
Skagerrak/Kattegat (S13)	Norwegian Trench	58°N 9°E	1100	●○	2-G	17 10⁻³, 0			Dale et al., 2008c
Skagerrak/Kattegat (S10)	Norwegian Trench	58°N 9°E	280	●○	2-G	27 10⁻³, 18 x 10⁻⁵			Dale et al., 2008c
			y⁻¹						
No biomass									
Kinetic-thermodynamic									
Theoretical model	Active site (theoretical)		18.3	●				●	Dale et al., 2008b
Theoretical model	Passive site (theoretical)		18.3					●	Dale et al., 2008b
Imposed rate profile									
Green Canyon	Gulf of Mexico	27°N 9°W						●	Ussler and Paull, 2008
Benguela Coastal Upwelling System (3703, 3714)	Namibian Shelf	22°S 12°E		○			●		Fossing et al., 2000
Benguela Coastal Upwelling System	Namibian Shelf	22°S 12°E							Riedinger et al., 2006
Congo Fan	Zaire Shelf	7°S 9°E							Zabel and Schulz, 2001
Argentine Basin and Urugay Margin	Southern Atlantic	37°S 52°W						●	Hensen et al., 2003
Argentine Basin and Urugay Margin	Southern Atlantic	37°S 52°W						●	Riedinger et al., 2005
Romanian Shelf (Station 7)	Black Sea	44°N 30°E			1st order SO₄⁻²				Jørgensen et al., 2001, 2004
Romanian Shelf (Station 4,5,6)	Black Sea	44°N 30°E			Rate Imposed				Jørgensen et al., 2001, 2004
Blake Ridge	Offshore South-Eastern US	31°N 75°W		●					Borowski et al., 2000
Amazon Fan	Brazilian Continental Shelf	5°N 47°W							Adler et al., 2000
Benguela Current	West African Margin	5°-32°S 12°E							Sivan et al., 2007
Aarhus Bay	Baltic Sea	57°N 10°E							Thomsen et al., 2001
Mass balance									
Saanich Inlet	West Coast North America	48°N 123°W							Devol, 1983
Saanich Inlet	West Coast North America	48°N 123°W			1 G	0.32			Murray et al., 1978
Cariaco Basin	Venezuelan Continental Shelf	10.5°N 65°W							Reeburgh, 1976

[a] If blank, no organic matter modelled; [b] only reported for G-models; [c] after Luff and Wallmann, 2003; [d] different rate constants used for sulfate reduction and methanogenesis; and [e] using AOM aggregate density of 0.5·10⁺⁸cm⁻³.

Only a handful of studies explicitly account for the role of bioenergetic limitations on AOM and associated reactions. Thermodynamic limitation may help explain the tailing of methane above the SMTZ in Skagerrak sediments (Dale et al., 2008c; Knab et al., 2008). Model predictions remain, however, largely theoretical because the field data on the distributions of reactive intermediates, in particular H_2, are scarce. The only RTM study that represents the functional biomasses in AOM dynamics (Dale et al., 2008b) indicates that temporal changes in the active biomass of methane oxidizers under changing environmental conditions may significantly affect the efficiency of the AOM barrier. This brings into question the use of the biomass-implicit AOM models in non-steady state environments (e.g. Haese et al., 2003; Luff and Wallmann, 2003; Linke et al., 2005; Arndt et al., 2009). Short-term changes in the fluid advection rates at seeps (e.g. Tryon and Brown, 2001) and bottom water temperature and, thus, reaction rates in coastal sediments (e.g. Dale et al. 2008a) suggest that non-steady state conditions may be a frequent feature in AOM settings. Nonetheless, without more observational data on the response of the resident microbial communities to changes in the environmental forcings, transient simulations remain difficult to validate.

All spatially-resolved models consider diffusive transport and more than half also include upward advection of solutes triggered by groundwater discharge, tectonic activity or dewatering processes. Fluid transport in heat convection cells may be significant around hydrothermal vents but, to our knowledge, has not been investigated for its impact on AOM dynamics. In settings without the externally-impressed fluid flow, the solute transport by sediment burial is often neglected because the flux is orders of magnitude less than diffusion (e.g. Fossing et al., 2000; Jørgensen et al., 2001, Arndt et al., 2006).

Although biologically induced mixing significantly impacts bio-geochemical activity just below the sediment–water interface, it is generally assumed to have only a limited, largely indirect effect on AOM in passive settings, because the SMTZ is usually located well below the mixed surface layer (Dale et al., 2009c). Therefore, it is not surprising that bioturbation and bioirrigation are only considered in a fourth of the studies in Table 5. Burrows and tubes in Namibian slope sediments, however, have been found to extend several meters below the seafloor and porewater irrigation could have a more direct effect on AOM in this particular environment (Fossing et al., 2000). In active settings where the SMTZ tends to be located close to the SWI, mixing by macrofauna can have a more direct effect on AOM dynamics. For instance, Calyptogena clam colonies irrigate the sediment at seep sites, making this the dominant transport process and source of sulfate for AOM (Wallmann et al., 1997). At sites with bacterial mats above seeps, non-local transport of sulfide, sulfate, nitrate and oxygen can also occur through the motility of large sulfur bacteria such as Beggiatoa (Jørgensen and Nelson, 2004), but this effect has not yet been fully explored in the context of AOM. Similarly, sulfide oxidation within microbial communities has largely been ignored, even though thick microbial mats are conspicuous at methane-rich sites where organoclastic sulfate reduction and AOM lead to high rates of sulfide production. At these sites, mass balance calculations (Linke et al., 2005; Sommer et al., 2006; Dale et al., 2009a) indicate that sulfide oxidation largely dominates the sulfate flux through the sediment–water interface and can impact the depth of the SMTZ.

About half (30) of the studies address AOM dynamics in hydrate-bearing sediments where methane can exist in dissolved, gaseous and solid form. Of these, 10 explicitly represent hydrate formation and dissociation with (1, Bhatnagar et al., 2008) or without (9) hydrate as a separate phase. Davie and Buffett (2001) and Haeckel et al. (2004) consider the role of the gas hydrate phase on methane transport but do not explicitly model the AOM rates. The remaining studies include the impact of hydrates on porewater advection rates and methane concentrations as a boundary condition. However, none addresses in detail the transport of gaseous methane into the GHSZ from below and the microbial dynamics within the GHSZ.

Studies on gas dynamics have largely been restricted to non-hydrate-bearing nearshore sediments where gas is produced within a few meters of the sea floor. Nine studies in Table 5 consider the influence of the gas phase on AOM, but only 2 represent methane gas as a separate phase (Mogollón et al., 2009; submitted for publication). Although gas transport is an important process supplying methane to the SMTZ, a unified theory for gas migration in unconsolidated muddy sediments is currently lacking. This is especially critical in the case of hechannelized flow, which allows large amounts of methane to escape to the water column in the gaseous and aqueous forms. In addition, field and laboratory observations of gas dynamics are scarce (Wever et al. 2006) and, therefore, hamper the development of empirically-derived models.

AOM modeling studies often do not explicitly represent organic matter decomposition and assume that methane is the sole electron donor for sulfate reduction. This is a reasonable assumption at sites with high rates of externally-impressed fluid advection or in passive settings where the SMTZ is tens of meters below the sea floor. In these cases, the influence of OM mineralization on AOM is minor (Borowski et al., 1996). Those modeling studies that account for organic matter degradation mostly use the G model. About one-third of these studies only consider one carbon pool, although the available evidence indicates that sedimentary organic matter reactivity is better represented when including multiple organic carbon pools. Multi-G models may include a labile ($k \approx 10^0 - 10^{-2}$ yr^{-1}), an intermediate ($k \approx 10^{-2} - 10^{-3}$ yr^{-1}) and/or a refractory pool ($k \approx < 10^{-3}$ yr^{-1}) of organic carbon. No AOM study has used the power law model of Middelburg (1989), although Wallmann et al. (2006b) combined this approach with Monod kinetic inhibition terms to describe organic matter degradation. Arndt et al. (2009) used the reactive continuum model to argue that the organic carbon-rich Cretaceous shales are dominated by highly unreactive organic matter pools with apparent rate constants that are lower than those predicted by the power law model.

The significant differences in model design and parameterization calls into question the transferability of AOM models and parameter values from one site to another. This is clearly shown in Fig. 12, which collates the values of the bimolecular rate constant for the AOM reported in Table 5. The range of values extends over 6 orders of magnitude and implies that this constant is a fitting parameter with limited mechanistic value. This is not surprising, as the bimolecular rate constant integrates the effects of a number of variables related to microbial community structure and abundance, bioenergetics and enzyme kinetics. These effects vary across settings and environmental conditions as evidenced by observational data (Treude et al., 2003) and theoretical considerations (Dale et al., 2008b). Despite their higher complexity, models based on a more solid mechanistic foundation typically yield narrower ranges of parameter values and are, therefore, applicable to a broader spectrum of AOM settings.

The need for sophistication over simplicity in AOM models is often guided by the nature of available observational data that allow one to identify the dominant reaction and transport processes. Table 6 presents an overview of experimental measurements that may help constrain and parameterize early diagenetic models with an emphasis on AOM. Even though not discussed in detail, the lower half of Table 6 lists a broader set of observations, which can be used to identify reaction and transport processes that impact AOM indirectly. The analytical measurements are ranked according to their relative importance in determining the depth-integrated AOM rate and the depth distribution of AOM. The highest priority is jointly assigned to the distributions of the methane and sulfate concentrations, which provide information on net transport fluxes to the SMTZ and, indirectly, net AOM rates. Sulfate reduction rates measured in $^{35}SO_4^{2-}$ incubations provide the next most important constraint, because they include not only sulfate reduction coupled to AOM but also organoclastic sulfate reduction. Distributions of dissolved inorganic carbon and alkalinity yield additional information on AOM and carbon mineralization rates (Wallmann et al., 2006b). In
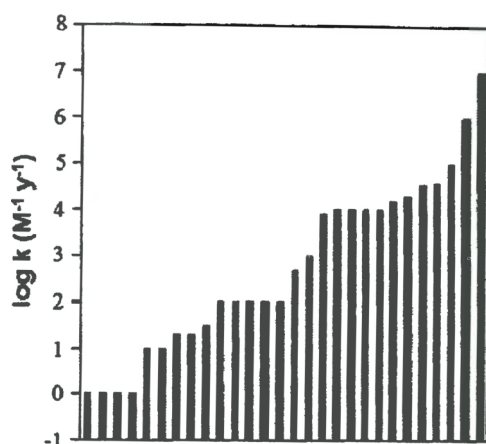
Fig. 12. Ranked histogram of individual bimolecular rate constants for AOM summarized in Table 5.

particular, the rate of methanogenesis can be derived from these porewater profiles, which is important for sediment cores where methane concentration measurements are affected by degassing during sampling. AOM rate profiles obtained by $^{14}CH_4$ tracer incubation experiments commonly show a high degree of scatter due to experimental artifacts (Alperin and Hoehler, 2009) and the natural heterogeneity of sediments (e.g. Treude et al., 2003), and are thus assigned a lower priority. Stable carbon isotope distributions are less prone to experimental artifacts and therefore provide more reliable constraints on AOM and methanogenesis. Stable isotope distributions could help reveal the occurrence of methanogenesis and AOM above the SMTZ (Parkes et al., 2007) where these processes are commonly assumed to be inhibited.

Table 6

Observational data ranked according to their usefulness to reactive transport models of AOM in sediments (upper half). Knowledge of the boundary conditions is implicitly assumed. The lower half of the table lists additional observations which are useful to constrain processes which are indirectly impacting AOM.

Rank	Step	Comment	Example
1=	CH_4 concentration	CH_4 flux to the SMTZ	Fossing et al. (2000)
1=	SO_4^{2-} concentration	SO_4^{2-} flux to the SMTZ	D'Hondt et al. (2002)
3	$^{35}SO_4^{2-}$ incubation	POC reactivity above SMTZ + AOM rate	Jørgensen (1978)
4	DIC concentration	POC reactivity above and below SMTZ + AOM rate	Dale et al. (2008a,b,c)
5	Total alkalinity	POC reactivity above and below SMTZ + AOM rate	Luff and Wallmann (2003)
6	$^{14}CH_4$ incubation	AOM rate	Treude et al. (2005)
7	^{13}DIC and $^{13}CH_4$ concentration	Methanogenesis + AOM rate	Alperin et al. (1988)
8	$^{14}Acetate$ and $14CO_2$ incubation	Direct determination of methanogenesis	Parkes et al. (2007)

Additional observations

ϕ	Volume conservation
$^{210}Pb_{xs}$ (+ others)	Sediment accumulation rate + bioturbation rate and depth
Cl^- concentration	Externally-impressed fluid advection
Br^- concentration	Bioirrigation rate and depth
Total oxygen uptake	POC reactivity + bioirrigation
NH_4^+ concentration	POC reactivity
H_2S concentration	Sulfate reduction + sulfide sinks
Fe^{2+} concentration	Sulfide sinks
Sedimentary S	Net sulfate reduction rate
Ca^{2+}, Mg^{2+} concentration	Carbonate dissolution + precipitation
Free gas depth and gas volume	Gas flux
Seismic profiles	Depth of free gas and/or hydrates

4. Global trends in AOM

Table 7 lists the 58 studies from Table 5 for which depth-integrated AOM rates (ΣAOM) are reported or could be calculated from the AOM rate profiles. The rates are ranked from highest to lowest together with selected environmental conditions including bathymetry, transport parameters (v_a, ω) and, where available, the particulate organic carbon (POC) deposition flux (F_{POC}). We also include qualitative information about the existence of hydrates, gas and microbial mats, irrespective of whether they were explicitly included in the corresponding models or not.

As can be seen in Fig. 13a a positive correlation ($r^2 = 0.89$) exists between log ΣAOM and log v_a at sites with externally-impressed fluid advection (see also, Luff and Wallmann, 2003; Aloisi et al., 2004a). Note that although gas transport may account for a non-negligible fraction of the methane fueling AOM (Torres et al., 2004), it is generally not considered in AOM models and therefore not included in the present analysis. Furthermore, the aqueous methane flux towards the SMTZ depends not only on v_a, but also on the dissolved methane concentration, whose upper limit is set by the in situ solubility. For instance, focusing on $v_a \approx 10$ cm yr^{-1}, sites at Hydrate Ridge (entries 9, 12, 15 and 25 in Table 7), where the water depth is ca. 800 m, have a mean ΣAOM which is 3 times larger than that of the comparatively shallow (26 m) Eckernförde Bay setting (entries 20 and 26). Thus, the dependence of the dissolved methane solubility on the water depth explains part of the observed scatter in Fig. 13a.

The number of available values of F_{POC} is insufficient to define a trend with ΣAOM, yet the importance of F_{POC} can be inferred indirectly from the data in Table 7. When all sites are considered, with or without pore fluid advection, a strong log–log correlation ($r^2 = 0.84$) is obtained between ΣAOM and the SMTZ depths (Fig. 13b). For active sites, the advection of methane-rich pore fluids decreases the depth of the STMZ and, as shown in Fig. 13a, leads to a sharp increase in ΣAOM. In the absence of fluid flow, the correlation is maintained, however, suggesting that the burial flux of the reactive organic matter below the zone of sulfate reduction is the external forcing with the largest effect on the SMTZ depth in passive settings. Given these considerations, the sites listed in Table 7 are categorized into active and passive settings and, based on the global relationship between F_{POC} and water depth (e.g. Middelburg et al., 1997), further subdivided into sites located below (>200 m) and above (<200 m) the shelf break. The latter classification assumes that the supply of reactive organic matter at the seafloor represents a primary control on the production of methane.

Sediments below the shelf break characterized by active fluid flow (ABSB, Fig. 14a,b) exhibit the highest mean ΣAOM value (6.8 mol m^{-2}yr^{-1}). Upward fluid flow rates at ABSB sites where the AOM process has been modeled range from 0.005 to 30 cm yr^{-1}. The advective methane flux at these sites is generally much larger than the organic carbon burial rate below the sulfate reduction zone (e.g. Sommer et al., 2006), which implies a minor role of organic matter degradation in controlling ΣAOM. Consequently, organic matter degradation has been ignored in almost all ABSB model applications, and the depth-integrated sulfate reduction rate (ΣSR) is entirely attributed to AOM. Due to upward fluid flow, the average depth of the SMTZ at ABSB sites is <50 cm (Fig. 14b).

Very few models have been applied to active sites above the shelf break (AASB), despite the widespread presence of pockmark-like structures along the coastline (Judd and Hovland, 2007). At AASB locations, fluid seepage driven by groundwater input from land can enhance the upward flux of methane. Based on the available studies, ΣAOM varies between 0.28 and 3 mol m^{-2}yr^{-1} with an average value on the order of 1 mol m^{-2}yr^{-1} (Fig. 14a, b). High sedimentation rates (0.1–1 cm yr^{-1}) and organic matter fluxes (1–4.6 mol m^{-2}yr^{-1}) lead to the rapid development of anaerobic conditions within the sediments. The average $\Sigma AOM/\Sigma SR$ ratio is about 70% (Table 7), and organoclastic sulfate reduction rates are elevated in the upper

Table 7

Ranking of depth-integrated AOM rates (ΣAOM) based on entries in Table 5 for which this information is available. Except if stated otherwise, ΣAOM values were directly taken from the given references. SMTZ depths, total sulfate-reduction (SR) rates and selected environmental conditions are also reported. Blank entries in the Table indicate that the information is missing in the original reference. Filled and empty circles denote the presence or absence of hydrates, gas and microbial mats, respectively. Entries in bold in the reference list indicate studies that have used the same model design to estimate more than one value of ΣAOM at nearby sites.

Site (core name)	Location	Integrated AOM rates (mol m^{-2} y^{-1})	SMTZ depth (cm)	Integrated total SR rates (mol m^{-2} yr^{-1})	Waterdepth (m)	v_s^e (cm y^{-1})	ω^f (cm y^{-1})	F_{OC}^g (mol m^{-2} y^{-1})	Hydrates	Gas	Mats	Type	Reference
Dvurechenskii mud volcano (MIC – 3)	Black Sea	17.2	2		2070	25	0.003-0.005	0	●		●		Wallmann et al. (2006a)
Hydrate Ridge	Cascadia Subduction Zone no CaCO₃ crust	10.92	3.5		775	30	0.0275	0	●		●		**Luff et al. (2004)**
Hydrate Ridge	Cascadia Subduction Zone no CaCO₃ crust	10.75	1.9	10.803	790	30	0.0275	0.55, 0.26	●		●		**Luff et al. (2005)**
Dvurechenskii mud volcano (MIC – 4)	Black Sea	10.2	2.5		2085	15	0.003-0.005	0	●		●		Wallmann et al. (2006a)
Hydrate Ridge	Cascadia Subduction Zone	9.25	2.5	9.78	790	10	0.0275	0.55, 0.26	●		●		Luff and Wallmann (2003)
Hydrate Ridge	Cascadia Subduction Zone	9.1	2			10		0.2	●		●		Zeebe (2007)
Dvurechenskii mud volcano (MIC – 5)	Black Sea	6.6	3		2089	8	0.003-0.005	0	●		●		Wallmann et al. (2006a)
Hydrate Ridge	Cascadia Subduction Zone with CaCO₃ crust	6.09	5		775	10	0.0275	0	●		●		**Luff et al. (2004)**
Anaximander Mountains	Eastern Mediteranean	6	14		1720	4	0.004	0	●		○		Haese et al. (2003)
Middle America Trench	Costa Rica Forearc	5.88	3.5		1000	10		0	●	●	●		Linke et al. (2005)
Hydrate Ridge (Beggiatoa 2)	Cascadia Subduction Zone	5.62	5		777	10	0.0275	0	●		●		Treude et al. (2003)
Hydrate Ridge (BIGO 4)	Cascadia Subduction Zone	5.51	3	5.48	778	20	0.0275	0.55, 0.26	●		●		Sommer et al. (2006)
Hydrate Ridge (Beggiatoa 1)	Cascadia Subduction Zone	4.85	3		777	0	0.0275	0	●		●		Treude et al. (2003)
Hydrate Ridge	Cascadia Subduction Zone	4.5	5	4.553	790	2	0.0275	0.55, 0.26	○		○		Luff et al. (2005)
Middle America Trench	Costa Rica Forearc	3.5	140		1020	5	0.03	0	●		○		Schmidt et al. (2005)
Eckernfoerde Bay (Pockmark)	Kiel Bight	3	5	3.3	26	10	0.6	4.6	○			AAS	Albert et al. (1998)
Anaximander Mountains	Eastern Mediteranean	3ᵃ	25			10	0.00001	0	●		○		Aloisi et al. (2004a)
Saanich Inlet	West Coast North America	2.46	25		225	ωᵈ	1.04ʰ	0	○	●	○	PAS	Murray et al. (1978)
Hikurangi Margin	New Zealand	2.2	5	2.6	700	14	0.16	1.2	●		○		Dale et al. (2010)
Saanich Inlet	West Coast North America	1.4	12		225	ω	ʰ	0	○	●	○	PAS	Devol et al. (1984)
Hydrate Ridge (BIGO 5)	Cascadia Subduction Zone	1.31	12.5	1.31	777	10	0.0275	0.55, 0.26	●		○		Sommer et al. (2006)
Eckernfoerde Bay (Pockmark)	Kiel Bight	1.1ᵇ	9ᵇ	1.24	25	10	0.6ʰ	1.8	○	●	○	AAS	**Mogollón et al. (submitted)**
Saanich Inlet	West Coast North America	0.955	18		225	0ᵉ	0	0	○	●	○	PAS	Devol (1983)
Congo Fan	Zaire Shelf	0.8	1550		4000	0	0.005	0	○		○		Zabel and Schulz (2001)
Eckernfoerde Bay (Acoustic Window)	Kiel Bight	0.5	30	1.2	26	3.5	0.6	2.3	○		○	AAS	Albert et al. (1998)
Green Canyon	Gulf of Mexico	0.5ᵇ	300		647	0	0.025ᵇ	0	●		○		Ussler and Paull (2008)
Eckernfoerde Bay (NRL)	Kiel Bight	0.426	30	1.14	26	1	0.6	2.3	○	●	○		Martens et al. (1998, 1999)
Aarhus Bay (M5)	Baltic Sea	0.41	150	2.98	15	ω	0.2	1.0, 0.23, 2.7	○	●	○		Dale et al. (2008a)
Eckernfoerde Bay (NRL)	Kiel Bight	0.39ᵇ	29ᵇ	0.55	25	1	0.6ʰ	0.9	○	●	○		**Mogollón et al. (submitted)**
Eckernfoerde Bay (NRL)	Kiel Bight	0.28	35	0.688	25	1	0.6	1.025	○	●	○		Mogollón et al., 2009

Benguela Coastal Upwelling System	*Namibian Shelf*	0.22	110	6.32	110	ω	0.34	7.0, 4.5, 1.6	o	•	•		Dale et al., 2009a
Cariaco Basin	Venezuelan Continental Shelf	0.142	-	0.158	40	1200	0	0.05	o	•	o		Reeburgh, 1976
Amazon Fan	Brazilian Continental Shelf	0.1[a]		400	40[b]	0	0.8	0	o		o		Blair and Aller, 1995
Skagerrak/Kattegat (S10)	Norwegian Trench	0.09	310	0.86	86	ω	0.5	2.69, 0.25	o	•	o		Dale et al., 2008c
Aarhus Bay (M1)	Baltic Sea	0.088	105-120	4.86	27	ω	0.02	4.5, 0, 2.5	o	•	o		Dale et al., 2008a
Benguela Coastal Upwelling System (3703)	Namibian Shelf	0.08	350	0.73	1373	0	0.05		o				Fossing et al., 2000
Derugin Bassin/ Sakhalin Island (SO178 13-6 KL)	Sea of Okhotsk	0.0785	270	0.2	713	ω	0.093		•		o		Wallmann et al., 2006b
Site 1040/1254	Costa Rica Forearc	0.074	40000		4312	0.4							Haeckel et al., 2006
Aarhus Bay	Baltic Sea	0.0621	185		16	0		0	o		o		Thomsen et al., 2001
Derugin Bassin/ Sakhalin Island (SO178 29-2 KL)	Sea of Okhotsk	0.059	380	0.14	771	ω	0.115		•		o		Wallmann et al., 2006b
Amazon Fan	Brazilian Continental Shelf	0.055[a]	400		3510	ω	0.0035	0	o		o		Adler et al., 2000
Benguela Coastal Upwelling System (3714)	Namibian Shelf	0.055	580	1.83	2065	0	0.05		o				Fossing et al., 2000
Derugin Bassin/ Sakhalin Island	Sea of Okhotsk	0.049	250		1700	0.14	0.011	0	•		o		Aloisi et al., 2004b
Derugin Bassin/ Sakhalin Island (LV28 20-2 SL)	Sea of Okhotsk	0.0454	285	0.15	685	ω	0.09		•		o		Wallmann et al., 2006b
Romanian Shelf (st 4)	Black Sea	0.041	180	0.237	130	0			o	o	o		Jørgensen et al., 2001, 2004
Romanian Shelf (st 5)	Black Sea	0.035	210	0.522	181	0			o	o	o		Jørgensen et al., 2001, 2004
Skagerrak/Kattegat (S13)	Norwegian Trench	0.033	100	1.14	361	ω	0.5	1.74, 0	o	•	o		Dale et al., 2008c
Benguela Current	West African Margin	0.03	5000	0.1	400 - 2200	ω	0.005 - 0.035		o		o		Sivan et al., 2007
Romanian Shelf (st 6)	Black Sea	0.03	250	0.27	396	0			o	o	o		Jørgensen et al., 2001, 2004
Romanian Shelf (st 7)	Black Sea	0.018	>350	0.27	1176	0			o	o	o		Jørgensen et al., 2001, 2004
Derugin Bassin/ Sakhalin Island (SO178 10-6 SL)	Sea of Okhotsk	0.016	980	0.048	613	ω	0.013		•		o		Wallmann et al., 2006b
Blake Ridge (ODP997)	Offshore South-Eastern US	0.0105	2200	0.013	2770	0.012	0.022		•		o		Wallmann et al., 2006b
Blake Ridge	Offshore South-Eastern US	0.004	2100	0.0114	2000- 3000	ω	0.0057	0	•		o		Borowski et al., 2000
North Atlantic (ODP leg162 site984A)	North Atlantic	0.0031	12500	0.0039	1650	0.005	0.0143[h]	$2.9\ 10^{-3}$	o	o	o		Maher et al., 2006
Derugin Bassin/ Sakhalin Island (LV28 2-4 SL)	Sea of Okhotsk	0.000467		0.019	1265	ω	0.01		•		o		Wallmann et al., 2006b
Derugin Bassin/ Sakhalin Island (SO178 3-4 KAL)	Sea of Okhotsk	0.000205		0.0063	1602	ω	0.01		•		o		Wallmann et al., 2006b
Demerara Rise (site 1258)	Equatorial Atlantic	0.00003-0.00016[a]	16000-40000	0.00003-0.00016	2450-3200	0	$0.67 - 1.5 \times 10^{-3}$		o	o	o		Arndt et al., 2009
Demerara Rise (site 1257-1260)	Equatorial Atlantic	0.00005[b]	15000-40000	0.00005	3200	0	$0.0 - 1.5 \times 10^{-3}$		o	o	o		Arndt et al., 2006

[a]Calculated from integration of the AOM rate profile; [b]time-average value from transient simulation or site-average value from multi-core modeling study; [c]positive upwards, [d]aqueous advection derived from sedimentation; [e]diffusion-only model, [f]positive downwards [g]multiple entries refer to the different G pools of the multi G model and [h]below the compacted layer.
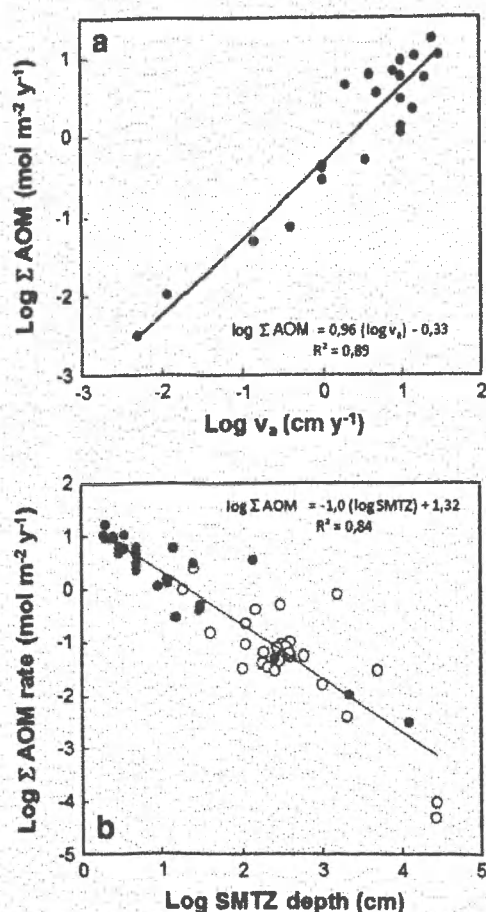
Fig. 13. (a) Log–log relationship of depth integrated AOM rates in active AOM settings as a function of fluid flow velocities; (b) log–log relationship of depth integrated AOM rates as a function of SMTZ depth for active (filled circles) and passive (open circles) sites.
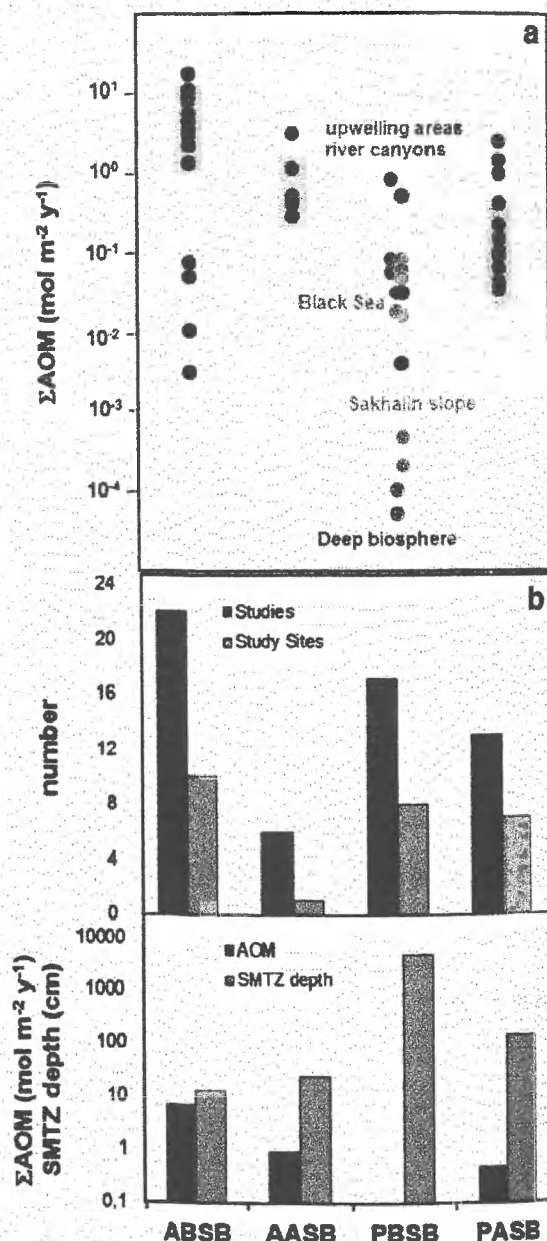

Fig. 14. Compilation of simulated AOM rates reported for the 4 different AOM environments. (a) Ranges of experimentally determined AOM rates (see Hinrichs and Boetius, 2002 for details) are denoted by the shaded grey bands; simulated mean AOM rates (black) and SMTZ depths (grey) for the different AOM environments. Mean values for ABSB sites exclude the 4 sites in Table 7 for which $v_a < 1$ cm yr^{-1}. (b) The number of modeling studies (black) and study sites (grey) are also reported.

sediment layers because of the shallow penetration of oxygen. As a result of the rapid rates of TEA consumption, methane concentrations commonly exceed the in situ solubility limit and gas advection can become an important mechanism of methane supply to the SMTZ. Consequently, the SMTZ tends to be located within the upper meter of sediment. The proximity of the SMTZ to the sediment–water interface may allow gaseous methane to escape to the water column.

In passive settings below the shelf break (PBSB), reported ΣAOM values vary between 5×10^{-5} and 0.8 mol m^{-2}yr^{-1} (Fig. 14a) with an average value of 0.1 mol m^{-2}yr^{-1} (Fig. 14b). PBSB sites thus show the largest variability in ΣAOM with a range covering 5 orders of magnitude. This is because several of the locations included in this category are not representative of globally averaged conditions at the sea floor, such as sites below upwelling areas or downslope from river canyons. PBSB settings are generally characterized by low rates of methane production deep in the sediment column and slow, diffusion-dominated transport. Modeling studies have addressed AOM in sediments receiving large inputs of organic matter, such as sediments from the Namibian upwelling system, the Sakhalin slope and the large Congo and Amazon alluvial fans. Here, large amounts of allochthonous and autochthonous organic matter are exported off the shelf and sustain the highest AOM rates quantified to date for PBSB sites. Water column anoxia also favors AOM by allowing more organic carbon to reach the methanic zone, a process observed for Black Sea sediments below the Romanian shelf. These higher rates are nevertheless one and two orders of magnitude lower than the mean values for AASB and ABSB sites, respectively. At the other end of the spectrum, very low rates have been derived for deeply buried Cretaceous black shale sequences where AOM is fueled by extremely slow rates of methano-genesis (Arndt et al., 2009). Based on the available data (Table 7), the contribution of AOM to total sulfate reduction is smaller at passive than at active sites (ΣAOM/ΣSR of about 40%).

Sediments deposited in passive settings above the shelf break (PASB) exhibit AOM rates (range: 3×10^{-2} to 2.5 mol m^{-2}yr^{-1}, average 0.5 mol m^{-2}yr^{-1}) that are generally higher than in passive settings below the shelf break, but lower than for the shallow active sites. The average SMTZ depth is also between the average values calculated for the PBSB and AASB sites (on average ≥ 1 m). The average ΣAOM/ΣSR is roughly half the value for the sites below the shelf break (Table 7). This preliminary analysis shows that despite the site-specific nature of the existing modeling studies on AOM, it is possible to use their results to identify global trends between ΣAOM and key environmental variables.

5. Challenges and open questions

Despite considerable progress achieved over the last 3 decades, current AOM models still involve various degrees of simplification that limit their transferability across time and space. One of the biggest challenges facing the next generation of RTMs will be the development of generalized biogeochemical reaction networks that apply to the entire spectrum of boundary conditions encountered at the seafloor. Here we identify further some of the outstanding challenges and open questions that should help direct future research and thus provide improved estimates of the global relevance of AOM and its evolution throughout Earth's history.

5.1. Organic matter degradation

More quantitative knowledge is required about the factors that influence organic matter mineralization, including the microbial community structure, the composition and oxidation state of the organic substrates, mineral–organic interactions, and redox conditions. The representation of these controls in RTMs should lead more general descriptions of organic matter decomposition in sediments.

5.2. Bioenergetics of AOM

Particularly important objectives are to reduce uncertainties in the minimum energy yields that microorganisms require to remain active and maintain cellular integrity, as well as to better constrain the chemical composition of the medium immediately surrounding microbes in aquatic sediments. This information is essential to determine the catabolic energy yields in AOM communities and to incorporate these in models for the growth and decay of microbial biomasses.

5.3. Representation of the biophase

The inclusion of the biophase is of particular relevance for model transferability and for addressing AOM dynamics under changing environmental conditions. The improvements to existing RTMs include the explicit representation of (1) microbial attachment and detachment processes between porewater and sediment particles, and (2) the microbial structure within biofilms and methane-oxidizing consortia. The scaling of interactions at the cellular level up to that of the macroscale fluxes and transformations remains a central challenge in the AOM studies.

5.4. Multi-phase dynamics

Full integration of the three methane phases into the comprehensive biogeochemical models of AOM is largely lacking, due in part to the fundamentally different space (and time) scales at which the phase transition and reactive processes occur. Large uncertainties also remain concerning the exact mechanisms of gas formation, migration and dissolution in unconsolidated sediments, especially when channelized flow occurs. In this context, the process-oriented field and laboratory observations of gas dynamics within marine sediments are urgently needed. These aspects are critical for a robust quantification of the efficiency of the AOM methane sink.

5.5. Regional and global upscaling

As global data sets and empirically-derived relationships for boundary conditions along the ocean hypsometry become available, RTM applications are no longer confined to local sampling sites. Global and regional RTM applications, however may not fully account for the effects of sediment heterogeneity on integrated biogeochemical fluxes and transformations. Moreover, much work remains to be done to adequately

represent the fundamental drivers of benthic dynamics. For instance, the uncertainties in the fluxes and biodegradability of organic matter, and in the size of the methane hydrate and gas reservoirs over large spatial scales seriously interferes with the global scale estimations of the methane fluxes and AOM rates. This is even more severe with regard to the paleoceanographic applications where observational evidence to constrain boundary conditions can only be gathered indirectly using biogeochemical proxies. Non-invasive methods that allow remote quantification of AOM through, for example, seismic surveying of the sea floor coupled with GIS technology, provide a promising avenue for methane budgeting on the regional scale. There is also a further need to couple benthic RTMs with regional and global scale general circulation models of the coupled carbon–climate system. In addition to inherent technical difficulties, this coupling is hampered by the fundamentally different characteristic time scales of the atmosphere, ocean and benthic dynamics. It is nevertheless of crucial importance to quantify the potential role of sea floor methane on the evolution of the earth's climate during the forthcoming centuries.

References

Abell, J., Laverman, A.M., Van Cappellen, P., 2009. Bioavailability of organic matter in a freshwater estuarine sediment: long-term degradation experiments with and without nitrate supply. Biogeochemistry 94, 256–271.
Adler, M., Hensen, C., Kasten, S., Schulz, H.D., 2000. Computer simulation of deep sulfate reduction in sediments of the Amazon Fan. International Journal of Earth Sciences 88, 641–654.
Albert, D.B., Martens, C.S., Alperin, M.J., 1998. Biogeochemical processes controlling methane in gassy coastal sediments—part 2: groundwater flow control of acoustic turbidity in Eckernförde Bay Sediments. Continental Shelf Research 18, 1771–1793.
Algar, C.K., Boudreau, B.P., 2009. Transient growth of an isolated bubble in muddy, fine-grained sediments. Geochimica et Cosmochimica Acta 73, 2581–2591.
Aloisi, G., Wallmann, K., Haese, R.R., Saliège, J.-F., 2004a. Chemical, biological and hydrological controls on the C content of cold seep carbonate crusts: numerical modeling and implications for convection at cold seeps. Chemical Geology 213, 359–383.
Aloisi, G., Wallmann, K., Bollwerk, S.M., Derkachev, A., Bohrmann, G., Suess, E., 2004b. The effect of dissolved barium on biogeochemical processes at cold seeps. Geochimica et Cosmochimica Acta 68, 1735–1748.
Alperin, M.J., Hoehler, T.M., 2009. Anaerobic methane oxidation by archaea/sulfate-reducing bacteria aggregates: 1. Thermodynamic and physical constraints. American Journal of Science 309, 869–957.
Alperin, M.J., Reeburgh, W.S., Whiticar, M.J., 1988. Carbon and hydrogen isotope fractionation resulting from anaerobic oxidation of methane. Global Biogeochemical Cycles 2, 279–288.
Alperin, M.J., Albert, D.B., Martens, C.S., 1994. Seasonal variations in production and consumption rates of dissolved organic carbon in an organic-rich sediment. Geochimica et Cosmochimica Acta 58, 4909–4930.
Alperin, M.J., Suayah, I.B., Benninger, L.K., Martens, C.S., 2002. Modern organic carbon burial fluxes, recent sedimentation rates, and particle mixing rates from the upper continental slope near Cape Hatteras, North Carolina (USA). Deep-Sea Research II 49, 4645–4665.
Amend, J.P., Plyasunov, A.V., 2001. Carbohydrates in thermophile metabolism: Calculation of the standard molal thermodynamic properties of aqueous pentoses and hexoses at elevated temperatures and pressures. Geochimica et Cosmochimica Acta 65, 3901–3917.
Anderson, A.L., Abegg, F., Hawkins, J.A., Duncan, M.E., Lyons, A.P., 1998. Bubble populations and acoustic interaction with the gassy floor of Eckernfoerde Bay. Continental Shelf Research 18, 1807–1838.
Archer, D., Buffett, B., Brovkin, V., 2008. Ocean methane hydrates as a slow tipping point in the global carbon cycle. Proceedings of the National Academy of Sciences of the United States of America. doi:10.1073/pnas.0800885105.

Arndt, S., Brumsack, H.J., Wirtz, K.W., 2006. Cretaceous black shales as active bioreactors: a biogeochemical model for the deep biosphere encountered during ODP Leg 207 (Demerara Rise). Geochimica et Cosmochimica Acta 70, 408–425.

Arndt, S., Hetzel, A., Brumsack, H.J., 2009. Evolution of organic matter degradation in Cretaceous black shales inferred from authigenic barite: a reaction-transport model. Geochimica et Cosmochimica Acta 73, 2000–2022.

Arnosti, C., 2004. Speed bumps and barricades in the carbon cycle: substrate structural effects on carbon cycling. Marine Chemistry 92, 263–273.

Arnosti, C., Holmer, M., 1999. Carbohydrate dynamics and contributions to the carbon budget of an organic-rich coastal sediment. Geochimica et Cosmochimica Acta 63, 393–403.

Audet, D.M., 1995. Modeling of porosity evolution and mechanical compaction of calcareous sediments. Sedimentology 42, 355–373.

Barnes, R.O., Goldberg, E.D., 1976. Methane production and consumption in anoxic marine sediments. Geology 4, 297–300.

Beal, E.J., House, C.H., Orphan, V.J., 2009. Manganese- and iron-dependent marine methane oxidation. Science 325, 184–187.

Bear, J., 1972. Dynamics of Fluids in Porous Media. American Elsevier, New York. 757 pp.

Berner, R.A., 1980. Early Diagenesis: A Theoretical Approach. Princeton University Press, Princeton. 241 pp.

Best, A.I., Richardson, M.D., Boudreau, B.P., Judd, A.G., Leifer, I., Lyons, A.P., Martens, C.S., Orange, D.L., Wheeler, S.J., 2006. Shallow seabed methane gas could pose coastal hazard. Eos Transactions 87, 213.

Bhatnagar, G., Chapman, W.G., Dickens, G.R., Dugan, B., Hirasaki, G.J., 2007. Generalization of gas hydrate distribution and saturation in marine sediments by scaling of thermodynamic and transport processes. American Journal of Science 307, 861–900.

Bhatnagar, G., Chapman, W.G., Dickens, G.R., Dugan, B., Hirasaki, G.J., 2008. Sulfate-methane transition as a proxy for average methane hydrate saturation in marine sediments. Geophysical Research Letters 35, L03611. doi:10.1029/2007GL032500.

Blair, N.E., Aller, R.C., 1995. Anaerobic methane oxidation on the Amazon shelf. Geochimica et Cosmochimica Acta 59, 3707–3715.

Boetius, A., Ravenschlag, K., Schubert, C.J., Rickert, D., Widdel, F., Gieseke, A., Amann, R., Jørgensen, B.B., Witte, U., Pfannkuche, O., 2000. A marine microbial consortium apparently mediating anaerobic oxidation of methane. Nature 407, 623–626.

Bohrmann, G., Torres, M.E., 2006. Gas hydrates in marine sediments, In: Schulz, H.D., Zabel, M. (Eds.), Marine Geochemistry, 2nd ed. Springer-Verlag, Berlin, pp. 271–309.

Borowski, W.S., Paull, C.K., Ussler III, W., 1996. Marine pore-water sulfate profiles indicate in situ methane flux from underlying gas hydrate. Geology 24, 655–658.

Borowski, W.S., Paull, C.K., Ussler III, W., 1999. Global and local variations of interstitial sulfate gradients in deep-water, continental margin sediments: Sensitivity to underlying methane and gas hydrates. Marine Geology 159, 131–154.

Borowski, W.S., Hoehler, T.M., Alperin, M.J., Rodriguez, N.M., Paull, C.K., 2000. In: Paull, C.K., Matsumoto, R., Wallace, P.J., Dillon, W.P. (Eds.), Significance of anaerobic methane oxidation in methane-rich sediments overlying the Blake Ridge gas hydrates: Proceedings of the Ocean Drilling Program, Scientific Results, 164, pp. 87–99.

Boudreau, B.P., 1984. On the equivalence of nonlocal and radial-diffusion models for porewater irrigation. Journal of Marine Research 42, 731–735.

Boudreau, B.P., 1997. Diagenetic Models and Their Implementation: Modelling Transport and Reactions in Aquatic Sediments. Springer-Verlag, Berlin. 414 pp.

Boudreau, B.P., Ruddick, B.R., 1991. On a reactive continuum representation of organic matter diagenesis. American Journal of Science 291, 507–538.

Boudreau, B.P., Algar, C., Johnson, B.D., Croudace, I., Reed, A., Furukawa, Y., Dorgan, K.M., Jumars, P.A., Grader, A.S., Gardiner, B.S., 2005. Bubble growth and rise in soft sediments. Geology 33, 517–520.

Brüchert, V., Arnosti, C., 2003. Anaerobic carbon transformation: experimental studies with flow-through cells. Marine Chemistry 80, 171–183.

Brüchert, V., Jørgensen, B.B., Neumann, K., Riechmann, D., Schlösser, M., Schulz, H., 2003. Regulation of bacterial sulfate reduction and hydrogen sulfide fluxes in the central namibian coastal upwelling zone. Geochimica et Cosmochimica Acta 67, 4505–4518.

Buffett, B., Archer, D., 2004. Global inventory of methane clathrate: sensitivity to changes in the deep ocean. Earth and Planetary Science Letters 227, 185–199.

Burdige, D.J., Gardner, K.G., 1998. Molecular weight distribution of dissolved organic carbon in marine sediment pore waters. Marine Chemistry 62, 45–64.

Burdige, D.J., Skoog, A., Gardner, K., 2000. Dissolved and particulate carbohydrates in contrasting marine sediments. Geochimica et Cosmochimica Acta 64, 1029–1041.

Caldwell, S.L., Laidler, J.R., Brewer, E.A., Eberly, J.O., Sandborgh, S.C., Colwell, F.S., 2008. Anaerobic oxidation of methane: mechanisms, bioenergetics, and the ecology of associated microorganisms. Environmental Science & Technology 42, 6791–6799.

Canavan, R.W., Slomp, C.P., Jourabchi, P., Van Cappellen, P., Laverman, A.M., van den Berg, G.A., 2006. Organic matter mineralization in sediment of a coastal freshwater lake and response to salinization. Geochimica et Cosmochimica Acta 70, 2836–2855.

Catling, D.C., Claire, M.W., Zahnle, K.J., 2007. Anaerobic methanotrophy and the rise of oxygen. Philosophical Transactions of the Royal Society A 365, 1867–1888.

Claypool, G.E., Kaplan, I.R., 1974. The origin and distribution of methane in marine sediments. In: Kaplan, I.R. (Ed.), Natural Gases in Marine Sediments. Plenum, New York, pp. 99–139.

Dale, A.W., Regnier, P., Van Cappellen, P., 2006. Bioenergetic controls on anaerobic oxidation of methane (AOM) in coastal marine sediments: a theoretical analysis. American Journal of Science 306, 246–294.

Dale, A.W., Aguilera, D.R., Regnier, P., Fossing, H., Knab, N.J., Jørgensen, B.B., 2008a. Seasonal dynamics of the depth and rate of anaerobic oxidation of methane in Aarhus Bay (Denmark) sediments. Journal of Marine Research 66, 127–155.

Dale, A.W., Van Cappellen, P., Aguilera, D.R., Regnier, P., 2008b. Methane efflux from marine sediments in passive and active margins: estimations from bioenergetic reaction-transport simulations. Earth and Planetary Science Letters 265, 329–344.

Dale, A.W., Regnier, P., Knab, N.J., Jørgensen, B.B., Van Cappellen, P., 2008c. Anaerobic oxidation of methane (AOM) in marine sediments from the Skagerrak (Denmark): II. Reaction-transport modelling. Geochimica et Cosmochimica Acta 72, 2880–2894.

Dale, A.W., Brüchert, V., Alperin, M., Regnier, P., 2009a. An integrated sulfur isotope model for Namibian shelf sediments. Geochimica et Cosmochimica Acta 73, 1924–1944.

Dale, A.W., Regnier, P., Van Cappellen, P., Fossing, H., Jensen, J.B., Jørgensen, B.B., 2009b. Remote quantification of methane fluxes in gassy marine sediments through seismic survey. Geology 37, 235–238.

Dale, A.W., Sommer, S., Haeckel, M., Wallmann, K., Linke, P., Wegener, G., Pfannkuche, O., 2010. Pathways and regulation of carbon, sulfur and energy transfer in marine sediments overlying methane gas hydrates on the Opouawe Bank (New Zealand). Geochimica et Cosmochimica Acta 74, 5763–5784.

Davie, M.K., Buffett, B.A., 2001. A numerical model for the formation of gas hydrate below the seafloor. Journal of Geophysical Research 106 (B1), 497–514.

Devol, A.H., 1983. Methane oxidation rates in the anaerobic sediments of Saanich Inlet. Limnology and Oceanography 28, 738–742.

Devol, A.H., Anderson, J.J., Kuivila, K., Murray, J.W., 1984. A model for coupled sulphate reduction and methane oxidation in the sediments of Saanich Inlet. Geochimica et Cosmochimica Acta 48, 993–1004.

D'Hondt, S., Rutherford, S., Spivack, A.J., 2002. Metabolic activity of subsurface life in deep-sea sediments. Science 295, 2067–2070.

D'Hondt, S., Jørgensen, B.B., Miller, D.J., Batzke, A., Blake, R., Cragg, B.A., Cypionka, H., Dickens, G.R., Ferdelman, T., Hinrichs, K.-U., Holm, N.G., Mitterer, R., Spivack, A., Wang, G., Bekins, B., Engelen, B., Ford, K., Gettemy, G., Rutherford, S.D., Sass, H., Skilbeck, C.G., Aiello, I.W., Guerin, G., House, C.H., Inagaki, F., Meister, P., Naehr, T., Niitsuma, S., Parkes, R.J., Schippers, A., Smith, D.C., Teske, A., Wiegel, J., Padilla, C.N., Solis Acosta, J.L., 2004. Distributions of microbial activities in deep subseafloor sediments. Science 306, 2216–2221.

Duan, Z., Moller, N., Greenberg, J., Weare, J.H., 1992. The prediction of methane solubility in natural waters to high ionic strength from 0 degrees to 250 degrees and from 0 to 1600 bar. Geochimica et Cosmochimica Acta 56, 1451–1460.

Emeis, K.C., Brüchert, V., Currie, B., Endler, R., Ferdelman, T., Kiessling, A., Leipe, T., Noli-Peard, K., Struck, U., Vogt, T., 2004. Shallow gas in shelf sediments of the Namibian coastal upwelling ecosystem. Continental Shelf Research 24, 627–642.

Ferdelman, T.G., Lee, C., Pantoja, S., Harder, J., Bebout, B.M., Fossing, H., 1997. Sulfate reduction and methanogenesis in a Thioploca-dominated sediment off the coast of Chile. Geochimica et Cosmochimica Acta 61, 3065–3079.

Flemings, P.B., Liu, X.L., Winters, W.J., 2003. Critical pressure and multiphase flow in Blake Ridge gas hydrates. Geology 31, 1057–1060.

Fossing, H., Gallardo, V.A., Jørgensen, B.B., Hüttel, M., Nielsen, L.P., Schulz, H., Canfield, D.E., Glud, R.N., Gundersen, J.K., Küver, J., Ramsing, N.B., Teske, A., Thamdrup, B., Ulloa, O., 1995. Concentration and transport of nitrate by the mat-forming sulphur bacterium Thioploca. Nature 274, 713–715.

Fossing, H., Ferdelman, T.G., Berg, P., 2000. Sulfate reduction and methane oxidation in continental margin sediments influenced by irrigation (South-East Atlantic off Namibia). Geochimica et Cosmochimica Acta 64, 897–910.

Gardiner, B.S., Boudreau, B.P., Johnson, B.D., 2003. Growth of disk-shaped bubbles in sediments. Geochimica et Cosmochimica Acta 67, 1485–1494.

Haeckel, M., 2006. In: Morris, J.D., Villinger, H.W., Klaus, A. (Eds.), A transport-reaction model of the hydrological systems of the Costa Rica subduction zone: Proceedings of the Ocean Drilling Programme, Scientific Results, 205.

Haeckel, M., Suess, E., Wallmann, K., Rickert, D., 2004. Rising methane gas bubbles form massive hydrate layers at the seafloor. Geochimica et Cosmochimica Acta 68, 4335–4345.

Haeckel, M., Boudreau, B.P., Wallmann, K., 2007. Bubble-induced porewater mixing: a 3-D model for deep porewater irrigation. Geochimica et Cosmochimica Acta 71, 5135–5154.

Haese, R.R., Meile, C., Van Cappellen, P., De Lange, G.J., 2003. Carbon geochemistry of cold seeps: methane fluxes and transformation in sediments from Kazan mud volcano, eastern Mediterranean Sea. Earth and Planetary Science Letters 212, 361–375.

Halbach, P., Holzbecher, E., Reichel, Th., Moche, R., 2004. Migration of the sulphate-methane reaction zone in the gas sediments of the Sea of Marmara—can this mechanism be tectonically induced? Chemical Geology 205, 73–82.

Hee, C.A., Pease, T.K., Alperin, M.J., Martens, C.S., 2001. Dissolved organic carbon production and consumption in anoxic marine sediments: a pulsed-tracer experiment. Limnology and Oceanography 46, 1908–1920.

Helgeson, H.C., Delany, J.M., Nesbitt, H.W., Bird, D.K., 1978. Summary and critique of the thermodynamic properties of rock-forming minerals. American Journal of Science 278, 1–229.

Hensen, C., Wallmann, K., 2005. Methane formation at Costa Rica continental margin—constraints for gas hydrate inventories and cross-décollement fluid flow. Earth and Planetary Science Letters 235, 41–60.

Hensen, C., Zabel, M., Pfeifer, K., Schwenk, T., Kasten, S., Riedinger, N., Schulz, H.D., Boetius, A., 2003. Control of sulfate pore-water profiles by sedimentary events and the significance of anaerobic oxidation of methane for the burial of sulfur in marine sediments. Geochimica et Cosmochimica Acta 67, 2631–2647.

Hinrichs, K.U., Boetius, A., 2002. The anaerobic oxidation of methane: new insights in microbial ecology and biogeochemistry. In: Wefer, G., Billett, D., Hebbeln, D., Jørgensen, B.B., Schlüter, M., Van Weering, T. (Eds.), Ocean Margin Systems. Springer-Verlag Berlin Heidelberg, pp. 457–477.

Hinrichs, K.U., Hayes, J.M., Sylva, S.P., Brewer, P.G., DeLong, E.F., 1999. Methane-consuming archaebacteria in marine sediments. Nature 398, 802–805.

Hoehler, T.M., 2004. Biological energy requirements as quantitative boundary conditions for life in the subsurface. Geobiology 2, 205–215.

Hoehler, T.M., Alperin, M.J., Albert, D.B., Martens, C.S., 1994. Field and laboratory studies of methane oxidation in an anoxic marine sediment—evidence for a methanogen–sulfate reducer consortium. Global Biogeochemical Cycles 8, 451–463.

Iversen, N., Jørgensen, B.B., 1985. Anaerobic methane oxidation rates at the sulphate–methane transition in marine sediments from Kattegat and Skagerrak (Denmark). Limnology and Oceanography 30, 944–955.

Jensen, M.M., Holmer, M., Thamdrup, B., 2005. Composition and diagenesis of neutral carbohydrates in sediments of the Baltic–North Sea transition. Geochimica et Cosmochimica Acta 69, 4085–4099.

Jin, Q., Bethke, C.M., 2005. Predicting the rate of microbial respiration in geochemical environments. Geochimica et Cosmochimica Acta 69, 1133–1143.

Johnson, J.W., Oelkers, E.H., Helgeson, H.C., 1992. SUPCRT92—a software package for calculating the standard molal thermodynamic properties of minerals, gases, aqueous species, and reactions from 1 bar to 5000 bar and 0 °C to 1000 °C. Computers and Geoscience 18, 899–947.

Jørgensen, B.B., 1977. The sulfur cycle of a coastal marine sediment (Limfjorden, Denmark). Limnology and Oceanography 22, 814–832.

Jørgensen, B.B., 1978. A comparison of methods for the quantification of bacterial sulfate reduction in coastal marine sediments. II Calculation from mathematical models. Geomicrobiology Journal 1, 29–47.

Jørgensen, B.B., Kasten, S., 2006. Sulfur cycling and methane oxidation. In: Schulz, H.D., Zabel, M. (Eds.), Marine Geochemistry, 2nd ed. Springer-Verlag, Berlin, pp. 271–309.

Jørgensen, B.B., Nelson, D.C., 2004. In: Amend, J.P., Edwards, K.J., Lyons, T.W. (Eds.), Sulfide oxidation in marine sediments: geochemistry meets microbiology: Sulfur Biogeochemistry—Past and Present: Geological Society of America Special Paper, 379, pp. 63–81.

Jørgensen, B.B., Weber, A., Zopfi, J., 2001. Sulfate reduction and anaerobic methane oxidation in Black Sea sediments. Deep-Sea Research I 48, 2097–2120.

Jørgensen, B.B., Böttcher, M.E., Holger, L., Neretin, L.N., Volkov, I.I., 2004. Anaerobic methane oxidation and a deep H2S sink generate isotopically heavy sulfides in Black Sea sediments. Geochimica et Cosmochimica Acta 68, 2095–2118.

Jourabchi, P., L'Heureux, I., Meile, C., Van Cappellen, P., 2010. Physical and chemical steady-state compaction in deep-sea sediments: role of mineral reactions. Geochimica et Cosmochimica Acta 74, 3494–3513.

Judd, A.G., Hovland, M., 2007. Seabed Fluid Flow: The Impact of Geology, Biology, and the Marine Environment. Cambridge University Press, Cambridge. 475 pp.

Knab, N.J., Dale, A.W., Lettmann, K., Fossing, H., Jørgensen, B.B., 2008. Thermodynamic and kinetic control on anaerobic oxidation of methane in marine sediments. Geochimica et Cosmochimica Acta 72, 3746–3757.

Knab, N.J., Cragg, B.A., Hornibrook, E.R.C., Holmkvist, L., Pancost, R.D., Borowski, C., Parkes, R.J., Jørgensen, B.B., 2009. Regulation of anaerobic methane oxidation in sediments of the Black Sea. Biogeosciences 6, 1505–1518.

Knittel, K., Boetius, A., 2009. Anaerobic oxidation of methane: progress with an unknown process. Annual Review of Microbiology 63, 311–334.

Komada, T., Reimers, C.E., Luther III, G.W., Burdige, D.J., 2004. Factors affecting dissolved organic matter dynamics in mixed-redox to anoxic coastal sediments. Geochimica et Cosmochimica Acta 68, 4099–4111.

Kotelnikova, S., 2002. Microbial production and oxidation of methane in deep subsurface. Earth Science Reviews 58, 367–395.

Kvenvolden, K.A., 1993. Gas hydrates—geological perspective and global change. Reviews of Geophysics 31, 173–187.

LaRowe, D.E., Helgeson, H.C., 2006a. Biomolecules in hydrothermal systems: calculation of the standard molal thermodynamic properties of nucleic-acid bases, nucleosides, and nucleotides at elevated temperatures and pressures. Geochimica et Cosmochimica Acta 70, 4680–4724.

LaRowe, D.L., Helgeson, H.C., 2006b. The energetics of metabolism in hydrothermal systems: calculation of the standard molal thermodynamic properties of magnesium-complexed adenosine nucleotides and NAD and NADP at elevated temperature and pressures. Thermochimica Acta 448, 82–106.

LaRowe, D.E., Helgeson, H.C., 2007. Quantifying the energetics of metabolic reactions in diverse biogeochemical systems: electron flow and ATP synthesis. Geobiology 5, 153–168.

LaRowe, D.E., Dale, A.W., Regnier, P., 2008. A thermodynamic analysis of the anaerobic oxidation of methane in marine sediments. Geobiology 6, 436–449.

Lavik, G., Stuehrrmann, T., Brüchert, V., Van der Plas, A., Mohrholz, V., Lam, P., Musmann, M., Fuchs, B.M., Amann, R., Lass, U., Kuypers, M.M.M., 2009. Detoxification of sulphidic African shelf waters by blooming chemolithotrophs. Nature 457, 581–584. doi:10.1038/nature07588.

Linke, P., Wallmann, K., Suess, E., Hensen, C., Rehder, G., 2005. In situ benthic fluxes from an intermittently active mud volcano at the Costa Rica convergent margin. Earth and Planetary Science Letters 235, 79–95.

Luff, R., Wallmann, K., 2003. Fluid flow, methane fluxes, carbonate precipitation and biogeochemical turnover in gas hydrate-bearing sediments at Hydrate Ridge, Cascadia Margin: numerical modeling and mass balances. Geochimica et Cosmochimica Acta 67, 3403–3421.

Luff, R., Wallmann, K., Aloisi, G., 2004. Numerical modeling of carbonate crust formation at cold vent sites: significance for fluid and methane budgets and chemosynthetic biological communities. Earth and Planetary Science Letters 221, 337–353.

Luff, R., Greinert, J., Wallmann, K., Klaucke, I., Suess, E., 2005. Simulation of long-term feedbacks from authigenic carbonate crust formation at cold vent sites. Chemical Geology 216, 157–174.

Maher, K., Steefel, C.I., DePaolo, D., Viani, B., 2006. The mineral dissolution rate conundrum: Insights from reactive transport modeling of U isotopes and pore fluid chemistry in marine sediments. Geochimica et Cosmochimica Acta 70, 337–363.

Martens, C.S., Berner, R.A., 1977. Interstitial water chemistry of anoxic Long Island Sound sediments. 1. Dissolved gases. Limnology and Oceanography 22, 10–25.

Martens, C.S., Klump, J.V., 1980. Biogeochemical cycling in an organic-rich coastal marine basin—I. Methane sediment-water exchange processes. Geochimica et Cosmochimica Acta 44, 471–490.

Martens, C.S., Albert, D.B., Alperin, M.J., 1998. Biogeochemical processes controlling methane in gassy coastal sediments—Part 1. A model coupling organic matter flux to gas production, oxidation and transport. Continental Shelf Research 18, 1741–1770.

Martens, C.S., Albert, D.B., Alperin, M.J., 1999. Stable isotope tracing of anaerobic methane oxidation in the gassy sediments of Eckernförde Bay, German Baltic Sea. American Journal of Science 299, 589–610.

Megonigal, J.P., Hines, M.E., Visscher, P.T., 2004. In: Schlesinger, W.H. (Ed.), Anaerobic metabolism: linkages to trace gases and aerobic processes. : Biogeochemistry, 8. Elsevier-Pergamon, Oxford, pp. 317–424.

Meile, C., Van Cappellen, P., 2003. Global estimates of enhanced solute transport in marine sediments. Limnology and Oceanography 48, 777–786.

Meile, C., Berg, P., Van Cappellen, P., Tuncay, K., 2005. Solute-specific pore water irrigation: implications for chemical cycling in early diagenesis. Journal of Marine Research 64, 601–621.

Meysman, F.J.R., Middelburg, J.J., Herman, P.M.J., Heip, C.H.R., 2003. Reactive transport in surface sediments. II. Media: an object-oriented problem-solving environment for early diagenesis. Computers and Geosciences 29, 301–318.

Meysman, F.J.R., Malyuga, V.S., Boudreau, B.P., Middelburg, J.J., 2006a. The influence of porosity gradients on mixing coefficients in sediments. Geochimica et Cosmochimica Acta 71, 961–973.

Meysman, F.J.R., Galaktionov, O.S., Gribsholt, B., Middelburg, J.J., 2006b. Bio-irrigation in permeable sediments: an assessment of model complexity. Journal of Marine Research 64, 589–627.

Middelburg, J.J., 1989. A simple rate model for organic matter decomposition in marine sediments. Geochimica et Cosmochimica Acta 53, 1577–1581.

Middelburg, J.J., Soetaert, K., Herman, P.M.J., 1997. Empirical relationships for use in global diagenetic models. Deep-Sea Research I 44, 327–344.

Mogollón, J.M., L'Heureux, I., Dale, A.W., Regnier, P., 2009. Methane gas-phase dynamics in marine sediments: a model study. American Journal of Science 309, 189–220.

Mogollón, J.M., Dale, A., L'Heureux, I., & Regnier, P. Seasonal controls on methane gas and anaerobic oxidation of methane in shallow marine sediments. Journal of Geophysical Research. submitted for publication.

Molins, S., Mayer, K.U., 2007. Coupling between geochemical reactions and multicomponent gas and solute transport in unsaturated media: a reactive transport modeling study. Water Resources Research 43, W05435. doi:10.1029/2006WR005206.

Molins, S., Mayer, K.U., Amos, R.T., Bekins, B.A., 2010. Vadose zone attenuation of organic compounds at a crude oil spill site—interactions between biogeochemical reactions and multicomponent gas transport. Journal of Contaminant Hydrology 112, 15–29.

Murray, J.W., Grundmanis, V., Smethie Jr., W.M., 1978. Interstitial water chemistry in the sediments of Saanich Inlet. Geochimica et Cosmochimica Acta 42, 1011–1026.

Nauhaus, K., Boetius, A., Kruger, M., Widdel, F., 2002. In vitro demonstration of anaerobic oxidation of methane coupled to sulphate reduction in sediment from a marine gas hydrate area. Environmental Microbiology 4, 296–305.

Nauhaus, K., Treude, T., Boetius, A., Krüger, M., Krüger, M., 2005. Environmental regulation of the anaerobic oxidation of methane: a comparison of ANME-I and ANME-II communities. Environmental Microbiology 7, 98–106.

Nauhaus, K., Albrecht, M., Elvert, M., Boetius, A., Widdel, F., 2007. In vitro cell growth of marine archaeal-bacterial consortia during anaerobic oxidation of methane with sulfate. Environmental Microbiology 9, 187–196.

Nihoul, J.C.J., 1976. Applied mathematical modelling in marine sciences. Applied Mathematical Modeling 1, 3–8.

Orcutt, B., Meile, C., 2008. Constraints on mechanisms and rates of anaerobic oxidation of methane by microbial consortia: process-based modeling of ANME-2 archaea and sulfate reducing bacteria interactions. Biogeosciences 5, 1587–1599.

Orphan, V.J., House, C.H., Hinrichs, K.U., McKeegan, K.D., DeLong, E.F., 2001. Methane-consuming archaea revealed by directly coupled isotopic and phylogenetic analysis. Science 293, 484–487.

Orphan, V.J., House, C.H., Hinrichs, K.U., McKeegan, K.D., DeLong, E.F., 2002. Multiple archaeal groups mediate methane oxidation in anoxic cold seep sediments. Proceedings of the National Academy of Sciences of the United States of America 99, 7663–7668.

Otte, S., Kuenen, J.G., Nielsen, L.P., Paerl, H.W., Zopfi, J., Schulz, H.N., Teske, A., Strotmann, B., Gallardo, V.A., Jørgensen, B.B., 1999. Nitrogen, carbon, and sulfur metabolism in natural Thioploca samples. Applied and Environmental Microbiology 65, 3148–3157.

Pallud, C., Van Cappellen, P., 2006. Kinetics of microbial sulfate reduction in estuarine sediments. Geochimica et Cosmochimica Acta 70, 1148–1162.

Parkes, R.J., Webster, G., Cragg, B.A., Weightman, A.J., Newberry, C.J., Ferdelman, T.G., Kallmeyer, J., Jørgensen, B.B., Aiello, I.W., Fry, J.C., 2005. Deep sub-seafloor prokaryotes stimulated at interfaces over geological time. Nature 436, 390–394.

Parkes, R.J., Cragg, B.A., Banning, N., Brock, F., Webster, G., Fry, J.C., Hornibrook, E., Pancost, R.D., Kelly, S., Knab, N., Jørgensen, B.B., Rinna, J., Weightman, A.J., 2007. Biogeochemistry and biodiversity of methane cycling in subsurface marine sediments (Skagerrak, Denmark). Environmental Microbiology 9, 1146–1161.

Raghoebarsing, A.A., Pol, A., van de Pas-Schoonen, K.T., Smolders, A.J.P., Ettwig, K.F., Rijpstra, W.I.C., Schouten, S., Sinninghe Damsté, J.S., Op den Camp, H.J.M., Jetten, M.S.M., Strous, M., 2006. A microbial consortium couples anaerobic methane oxidation to denitrification. Nature 440, 918–921.

Reagan, M.T., Moridis, G.J., 2008. Dynamic response of oceanic hydrate deposits to ocean temperature change. Journal of Geophysical Research 113, C12023. doi:10.1029/2008JC004938.

Reeburgh, W.S., 1976. Methane consumption in Cariaco Trench waters and sediments. Earth and Planetary Science Letters 28, 337–344.

Reeburgh, W.S., 1980. Anaerobic methane oxidation: rate depth distributions in Skan Bay sediments. Earth and Planetary Science Letters 47, 345–352.

Reeburgh, W.S., 2007. Oceanic methane biogeochemistry. Chemical Reviews 107, 486–513.

Regnier, P., O'Kane, J.P., Steefel, C.I., Vanderborght, J.P., 2002. Modeling complex multi-component reactive-transport systems: towards a simulation environment based on the concept of a knowledge base. Applied Mathematical Modelling 26 (9), 913–927.

Regnier, P., Dale, A.W., Pallud, C., van Lith, Y., Bonneville, S., Hyacinthe, C., Thullner, M., Laverman, A., Van Cappellen, P., 2005. Incorporating geomicrobial processes in subsurface reactive transport models. In: Nuetzmann, G., Viotti, P., Agaard, P. (Eds.), Reactive Transport in Soil and Groundwater: Processes and Models. Springer-Verlag, Berlin, pp. 107–126.

Riedinger, N., Pfeifer, K., Kasten, S., Lukina Garming, J.F., Vogt, C., Hensen, C., 2005. Diagenetic alteration of magnetic signals by anaerobic oxidation of methane related to a change in sedimentation rate. Geochimica et Cosmochimica Acta 69, 4117–4126.

Riedinger, N., Kasten, S., Gröger, J., Franke, C., Pfeifer, K., 2006. Active and buried authigenic barite fronts in sediments from the Eastern Cape Basin. Earth and Planetary Science Letters 241, 876–887.

Rittmann, B.E., VanBriesen, J.M., 1996. Microbiological processes in reactive modeling. In: Lichtner, P.C., Steefel, C.I., Oelkers, E.H. (Eds.), Reactive Transport in Porous Media. : Reviews in Mineralogy, 34. Mineralogical Society of America, Washington, pp. 311–334.

Robinson, R.A., Stokes, R.H., 1965. Electrolyte Solutions, 2nd ed. Butterworths, London, p. 571.

Schink, B., 1997. Energetics of syntrophic cooperation in methanogenic degradation. Microbiology and Molecular Biology Reviews 61, 262–280.

Schmidt, M., Hensen, C., Mörz, T., Müller, C., Grevemeyer, I., Wallmann, K., Mau, S., Kaul, N., 2005. Methane hydrate accumulation in "Mound 11" mud volcano, Costa Rica forearc. Marine Geology 216, 83–100.

Schowalter, T.T., 1979. Mechanics of secondary hydrocarbon migration and entrapment. American Association of Petroleum Geologists Bulletin 63 (5), 723–760.

Shock, E.L., Helgeson, H.C., 1988. Calculation of the thermodynamic and transport properties of aqueous species at high pressures and temperatures—correlation algorithms for ionic species and equation of state predictions to 5 kb and 1000 °C. Geochimica et Cosmochimica Acta 52, 2009–2036.

Shock, E.L., Helgeson, H.C., 1990. Calculation of the thermodynamic and transport properties of aqueous species at high pressures and temperatures—standard partial molal properties of organic species. Geochimica et Cosmochimica Acta 54, 915–945.

Shock, E.L., Helgeson, H.C., Sverjensky, D., 1989. Calculation of the thermodynamic and transport properties of aqueous species at high pressures and temperatures—standard partial molal properties of inorganic neutral species. Geochimica et Cosmochimica Acta 53, 2157–2183.

Shock, E.L., Sassani, D., Willis, M., Sverjensky, D., 1997. Inorganic species in geologic fluids: correlations among standard molal thermodynamic properties of aqueous ions and hydroxide complexes. Geochimica et Cosmochimica Acta 61, 907–950.

Sivan, O., Schrag, D.P., Murray, R.W., 2007. Rates of methanogenesis and methano-trophy in deep-sea sediments. Geobiology 5, 141–151.

Sommer, S., Pfannkuche, O., Linke, P., Luff, R., Greinert, J., Drews, M., Gubsch, S., Pieper, M., Poser, M., Viergutz, T., 2006. Efficiency of the benthic filter: Biological control of the emission of dissolved methane from sediments containing shallow gas hydrates at Hydrate Ridge. Global Biogeochemical Cycles 20, GB2019. doi:10.1029/2004GB002389.

Sørensen, K.B., Finster, K., Ramsing, N.B., 2001. Thermodynamic and kinetic require-ments in anaerobic methane oxidizing consortia exclude hydrogen, acetate, and methanol as possible electron shuttles. Microbial Ecology 42, 1–10.

Steefel, C.I., Lasaga, A.C., 1994. A coupled model for transport of multiple chemical species and kinetic precipitation/dissolution reactions with application to reactive flow in single phase hydrothermal systems. American Journal of Science 294, 529–592.

Steefel, C.I., MacQuarrie, K.T.B., 1996. Approaches to modeling of reactive transport in porous media. In: Lichtner, P.C., Steefel, C.I., Oelkers, E.H. (Eds.), Reactive Transport in Porous Media. : Reviews in Mineralogy, 34. Mineralogical Society of America, Washington, pp. 83–129.

Steefel, C.I., Maher, K., 2009. Fluid-rock interaction: a reactive transport approach. In: Oelkers, E.H., Schott, J. (Eds.), Thermodynamics and Kinetics of Water-Rock Interactions: Reviews in Mineralogy & Geochemistry, 70, p. 485–53.

Stöhr, M., Khalili, A., 2006. Dynamic regimes of buoyancy-affected two-phase flow in unconsolidated porous media. Physical Review E 27, 1–8.

Strous, M., Jetten, M.S.M., 2004. Anaerobic oxidation of methane and ammonium. Annual Review of Microbiology 58, 99–117.

Thomsen, T.R., Finster, K., Ramsing, N.B., 2001. Biogeochemical and molecular signatures of anaerobic methane oxidation in a marine sediment. Applied and Environmental Microbiology 67, 1646–1656.

Thullner, M., Van Cappellen, P., Regnier, P., 2005. Modeling the impact of microbial activity on redox dynamics in porous media. Geochimica et Cosmochimica Acta 69, 5005–5019.

Thullner, M., Regnier, P., Van Cappellen, P., 2007. Modeling microbially induced carbon degradation in redox-stratified subsurface environments: concepts and open questions. Geomicrobiology Journal 24, 139–155.

Thullner, M., Dale, A.W., Regnier, P., 2009. Global scale quantification of organic carbon degradation pathways in marine sediments: a reactive transport modeling approach. Geochemistry, Geophysics, Geosystems 10 (1). doi:10.1029/2009GC002484.

Tishchenko, P., Hensen, C., Wallmann, K., Wong, C.S., 2005. Calculation of the stability and solubility of methane hydrate in seawater. Chemical Geology 219, 37–52.

Torres, M.E., Wallmann, K., Tréhu, A.M., Bohrmann, G., Borowski, W.S., Tomaru, H., 2004. Gas hydrate growth, methane transport, and chloride enrichment at the southern summit of Hydrate Ridge, Cascadia margin off Oregon. Earth and Planetary Science Letters 226, 225–241.

Treude, T., Boetius, A., Knittel, K., Wallmann, K., Jørgensen, B.B., 2003. Anaerobic oxidation of methane above gas hydrates at Hydrate Ridge, NE Pacific Ocean. Marine Ecology Progress Series 264, 1–14.

Treude, T., Krüger, M., Boetius, A., Jørgensen, B.B., 2005. Environmental control on anaerobic oxidation of methane in the gassy sediments of Eckernförde Bay (German Baltic). Limnology and Oceanography 50, 1771–1786.

Tromp, T.K., Van Cappellen, P., Key, R.M., 1995. A global model for the early diagenesis of organic carbon and organic phosphorus in marine sediments. Geochimica et Cosmochimica Acta 59, 1259–1284.

Tryon, M.D., Brown, K.M., 2001. Complex flow patterns through Hydrate Ridge and their impact on seep biota. Geophysical Research Letters 28, 2863–2866.

Ussler III, W., Paull, C.K., 2008. Rates of anaerobic oxidation of methane and authigenic carbonate mineralization in methane-rich deep-sea sediments inferred from models and geochemical profiles. Earth and Planetary Science Letters 266, 271–287.

Valentine, D.L., 2002. Biogeochemistry and microbial ecology of methane oxidation in anoxic environments: a review. Antonie van Leeuwenhoek 81, 271–282.

Valentine, D.L., Reeburgh, W.S., 2000. New perspectives on anaerobic methane oxidation. Environmental Microbiology 2, 477–484.

Van Cappellen, P., Gaillard, J.F., 1996. Biogeochemical dynamics in aquatic sediments. In: Lichtner, P.C., Steefel, C.I., Oelkers, E.H. (Eds.), Reactive Transport in Porous Media. : Reviews in Mineralogy, 34. Mineralogical Society of America, Washington, pp. 335–376.

Van Cappellen, P., Wang, Y., 1996. Cycling of iron and manganese in surface sediments: a general theory for the coupled transport and reaction of carbon, oxygen, nitrogen, sulfur, iron, and manganese. American Journal of Science 296, 197–243.

van Genuchten, M.T., 1980. A closed-form equation for predicting the hydraulic conductivity of unsaturated soils. Soil Science Society of America Journal 44, 892–898.

VanBriesen, J.M., 2002. Evaluation of methods to predict bacterial yield using thermodynamics. Biodegradation 13, 171–190.

Wagman, D.D., Evans, W.H., Parker, V.B., Schumm, R.H., Halow, I., Bailey, S.M., Churney, K.L., Nuttall, R.L., 1982. The NBS tables of chemical thermodynamic properties-selected values for inorganic and C-1 and C-2 organic substances in SI units. Journal of Physical and Chemical Reference Data 11, 1–392.

Wallmann, K., Linke, P., Suess, E., Bohrmann, G., Sahling, H., Schlüter, M., Dählmann, A., Lammers, S., Greinert, J., von Mirbach, N., 1997. Quantifying fluid flow, solute mixing, and biogeochemical turnover at cold vents of the eastern Aleutian subduction zone. Geochimica et Cosmochimica Acta 61, 5209–5219.

Wallmann, K., Drews, M., Aloisi, G., Bohrmann, G., 2006a. Methane discharge into the Black Sea and the global ocean via fluid flow through submarine mud volcanoes. Earth and Planetary Science Letters 248, 544–559.

Wallmann, K., Aloisi, G., Haeckel, M., Obzhirov, A., Pavlova, G., Tishchenko, P., 2006b. Kinetics of organic matter degradation, microbial methane generation, and gas hydrate formation in anoxic marine sediments. Geochimica et Cosmochimica Acta 70, 3905–3927.

Wegener, G., Boetius, A., 2009. An experimental study on short-term changes in the anaerobic oxidation of methane in response to varying methane and sulfate fluxes. Biogeosciences 6, 867–876.

Westrich, J.T., Berner, R.A., 1984. The role of sedimentary organic matter in bacterial sulfate reduction: the G-model tested. Limnology and Oceanography 29, 236–249.

Wever, T.F., Abegg, F., Fiedler, H.M., Fechner, G., Stender, I.H., 1998. Shallow gas in the muddy sediments of Eckernförde Bay, Germany. Continental Shelf Research 18, 1715–1740.

Wever, Th.F., Lühder, R., Voß, H., Knispel, U., 2006. Potential environmental control of free shallow gas in the seafloor of Eckernförde Bay, Germany. Marine Geology 225, 1–4.

Xu, T., Pruess, K., 2001. Modeling multiphase flow and reactive geochemical in variably saturated fractured rocks: 1. Methodology. American Journal of Science 301, 16–33.

Zabel, M., Schulz, H.D., 2001. Importance of submarine landslides for non-steady state conditions in pore water systems—lower Zaire (Congo) deep-sea fan. Marine Geology 176, 87–99.

Zeebe, R.E., 2007. Modeling CO_2 chemistry, $d^{13}C$, and oxidation of organic carbon and methane in sediment porewater: implications for paleo-proxies in benthic foraminifera. Geochimica et Cosmochimica Acta 71, 3238–3256.

Zehnder, A.J.B., Brock, T.D., 1980. Anaerobic methane oxidation: occurrence and ecology. Applied and Environmental Microbiology 39, 194–204.